VERTICAL VARIATIONS IN THE MINERALOGY OF THE YICHUN TOPAZ–LEPIDOLITE GRANITE, JIANGXI PROVINCE, SOUTHERN CHINA

XIAO LONG HUANG

*Guangzhou Institute of Geochemistry, Chinese Academy of Sciences, Guangzhou, Wushan 510640,
China, and State Key Laboratory for Mineral Deposits Research, Department of Earth Sciences,
Nanjing University, Nanjing 210093, People's Republic of China*

RU CHENG WANG[§], XIAO MING CHEN, HUAN HU AND CHANG SHI LIU

*State Key Laboratory for Mineral Deposits Research, Department of Earth Sciences,
Nanjing University, Nanjing 210093, People's Republic of China*

ABSTRACT

The Yichun topaz–lepidolite granite is the latest and most evolved unit of the Yichun granitic complex, South China, and is well known by virtue of its unusual Ta–Nb–Li mineralization. A drill hole down to 300 m has intersected the granite from top to bottom, and revealed three petrographic zones: K-feldspar-rich facies in the lower part, albite-rich facies in the middle part, and Ab- and Kfs-rich facies in the upper part. Geochemically, the Yichun granite belongs to the phosphorus-rich type of rare-element-enriched granite. The phosphorus is concentrated in the feldspars, which contain up to 0.93 wt% P_2O_5. It is less enriched in feldspars in the middle part, where primary amblygonite is abundant. Principal accessory minerals include columbite–tantalite, cassiterite, zircon, and wodginite in all facies, and microlite in the middle facies. The composition of the columbite-group minerals corresponds to manganocolumbite and manganotantalite. Zircon contains mostly 4 to 8 wt% HfO_2, but the HfO_2 contents may reach up to 22 wt% at the rim. From the lower part to the middle part of the drill hole, the progressive increases in Ta/(Nb + Ta) of columbite and Ta-rich cassiterite, and in Hf content of zircon, are strongly suggestive of magmatic differentiation. On the other hand, in the upper part of the drill hole, the decrease in Ta/(Nb + Ta) of columbite and cassiterite, in Hf content of zircon, and the increase in Fe of lepidolite, and especially marked enrichment in Fe and W in columbite (5.76% FeO, 7.28% WO_3) at the uppermost part of the drill hole, indicate another environment at the final stage of crystallization of the granite, influenced by fluid probably derived from the surrounding mica schist.

Keywords: P-bearing feldspar, amblygonite, hafnian zircon, columbite–tantalite, cassiterite, electron-microprobe data, granite, Yichun, China.

SOMMAIRE

Le granite à topaze–lépidolite de Yichun, l'unité la plus tardive et la plus évoluée du complexe granitique de Yichun, du sud de la Chine, est bien connu à cause de son enrichissement inhabituel en Ta–Nb–Li. Un trou de forage de 300 m a intersecté ce granite pour révéler trois zones pétrographiques: faciès riche en feldspath potassique en profondeur, faciès albitique au milieu, et faciès enrichi dans les deux feldpaths vers le haut. En termes géochimiques, le granite de Yichun fait partie des granites enrichis en phosphore et en éléments rares. Le phosphore est concentré dans les feldspaths, qui contiennent jusqu'à 0.93% de P_2O_5 (poids). La concentration diminue dans le faciès du milieu, qui contient beaucoup d'amblygonite primaire. Parmi les principaux minéraux accessoires se trouvent columbite–tantalite, cassitérite, zircon, et wodginite dans tous les faciès, et microlite dans le faciès du milieu. La composition des minéraux du groupe de la columbite atteint le champ de la manganocolumbite et de la manganotantalite. Le zircon contient en général entre 4 et 8% de HfO_2 (poids), mais peut en contenir jusqu'à 22% en bordure des grains. En passant de la partie inférieure au milieu de l'intervalle échantillonné par le trou de forage, nous documentons une augmentation progressive en Ta/(Nb + Ta) de la columbite et de la cassitérite tantalifère, et de la teneur en Hf du zircon, qui témoigne d'une différenciation magmatique. En revanche, vers le haut de la section, la diminution en Ta/(Nb + Ta) de la columbite et de la cassitérite, en teneur en Hf du zircon, l'augmentation en Fe de la lépidolite, et l'enrichissement marqué en Fe et W de la columbite (5.76% FeO, 7.28% WO_3), surtout au sommet de la section, témoignent d'un milieu de cristallisation finale du granite influencé par une phase fluide, qui aurait été dérivée des schistes micacés encaissants.

(Traduit par la Rédaction)

Mots-clés: feldspath riche en phosphore, amblygonite, zircon hafnifère, columbite–tantalite, cassitérite, données de microsonde électronique, granite, Yichun, Chine.

§   *E-mail address*: rcwang@nju.edu.cn

INTRODUCTION

The Yichun (or Yashan) granitic complex, located in Jiangxi Province, southern China, is known for its unusual Ta–Nb–Li mineralization (exploited in deposit no. 414, Yin *et al.* 1995). Many studies have been made of its mineralogy, petrology, geochemistry, and metallogeny (*e.g.,* Lu *et al.* 1975, Pollard & Taylor 1991, Schwartz 1992, Yin 1988, Yin *et al.* 1993, 1995, Belkasmi *et al.* 1991, 2000). Yin *et al.* (1995) systematically described geological and geochemical characteristics of the Yichun Ta–Nb–Li deposit, and found that the granites show features of primary crystallization, with only minor modification by subsequent hydrothermal alteration. More recently, Belkasmi *et al.* (2000) made a detailed study of the Ta–Nb–Sn–W oxide minerals from this pluton, and discussed the magmatic-hydrothermal evolution of the host granites. Although the topaz–lepidolite granite is the most interesting unit at Yichun owing to its extreme fractionation and Ta–Nb–Li mineralization, it has not received due attention in the earlier investigations. In recent years, some exploratory drilling has been done in that unit. These bole holes, from 100 to 300 m deep, provide a rare opportunity to constrain the genesis of the granite. We report here the first detailed petrological study on a vertical section through the mineralized granite, and report details concerning the feldspars, the phosphates, zircon and Nb–Ta–Sn–Ti minerals in the topaz–lepidolite granite. Such information provides insight into both the magmatic crystallization and the post-magmatic stages of evolution of this most evolved unit of the Yichun complex.

GEOLOGICAL SETTING AND SAMPLING

The early Yanshanian (Jurassic) Yichun complex is situated in the Wugong Mountain migmatite–granite dome of the Jiangnan paleo-island arc of southern China. It has an outcrop area of approximately 9.5 km^2 (Yin *et al.* 1995). The complex consists of five intrusive units, which are, from oldest to youngest (Fig. 1): (1) medium- to coarse-grained protolithionite–muscovite granite, (2) fine-grained porphyritic muscovite granite, (3) medium-grained muscovite granite related to tungsten mineralization, (4) Li-mica granite, and (5) topaz–lepidolite granite with Ta–Nb–Li mineralization. Detailed petrographic information (modal compositions of minerals, textures, and grain sizes) is given in Yin *et al.* (1995). The Yichun complex represents an unusual example of Li–F-rich rare-metal granites with a complete succession from protolithionite granite to topaz–lepidolite granite. This study is focused particularly on the latest unit, which is hereafter named the Yichun topaz–lepidolite granite.

A 300-m-deep vertical hole was drilled in the Yichun topaz–lepidolite granite (Fig. 1). The drilling intersected this granite to a depth of about 43 m, which lies on top of the Li-mica granite (the fourth intrusive unit). Fifteen samples of the topaz–lepidolite granite are taken in the drill hole between –1 and –41.5 m (Fig. 1). Major rock-forming minerals include quartz, albite, K-feldspar and lepidolite in these fifteen samples. Petrographic studies demonstrate three facies in the topaz–lepidolite granite: (1) K-feldspar-rich facies in the lower part (samples Zk12–15, Fig. 1), (2) albite-rich facies in the middle part (samples Zk5–11, Fig. 1), and (3) albite- and K-feldspar-rich facies in the upper part (samples Zk1–4, Fig. 1). In all facies, the samples are porphyritic with phenocrysts of quartz, K-feldspar and topaz 1.5–3 mm in diameter, and a groundmass composed essentially of albite and lepidolite with lower amounts of quartz, topaz, and K-feldspar. The abundance of K-feldspar decreases from the lower part of the section to the middle part (15–30% and <5%, respectively), then increases in the upper part (7–22%). In a complementary way, albite increases from the lower part (20–30%) to the middle part (43–61%), then decreases in the upper part (30–45%). The proportion of quartz decreases noticeably from the lower part (34–54%) to the middle and upper parts (16–32%), whereas lepidolite increases from the lower part (6–10%) to the middle and upper parts (14–23%). Minor amounts of topaz (<5%) occur in all samples. The samples contain various kinds of accessory minerals, such as zircon, cassiterite, niobium–tantalum minerals, amblygonite (<3% in the middle part) and an apatite-group mineral. Most of the accessory minerals occur as inclusions in topaz, lepidolite, and the feldspars.

ANALYTICAL METHODS

The whole-rock composition of the samples was established by wet-chemical analysis at the Center Laboratory of Department of Earth Sciences, Nanjing University. Concentrations of the trace elements, including the rare-earth elements, were obtained by inductively coupled plasma – mass spectrometry (ICP–MS) at the Guangzhou Institute of Geochemistry, Chinese Academy of Sciences. Minerals were analyzed with a JEOL JXA 8800M electron microprobe at the State Key Laboratory for Mineral Deposits Research of Nanjing University. We used the following operating conditions (accelerating voltage, beam current, beam diameter): 15 kV, 10 nA, 1 μm for the feldspars and phosphates; 12 kV, 100 nA, 5 μm for lepidolite and topaz; 20 kV, 20 nA, 1 μm for Nb–Ta–Sn–U–Zr minerals. To measure the amount of phosphorus in feldspar, counting times of 60 s for phosphorus and a P-bearing orthoclase standard (0.49 wt% P_2O_5) was used. We used the ZAF program for data reduction.

GEOCHEMICAL TRENDS IN THE YICHUN BATHOLITH

Variations in major-element concentrations

In general, from the early to late units of the Yichun granite complex, the whole-rock SiO_2 contents decrease (on average, 75.1 wt% → 74.7% → 74.5% → 74.0% → 68.12%) in contrast to A/NKC values (molar) (on average, 1.25 → 1.26 → 1.28 → 1.24 → 1.40) (Y1 to Y5, respectively, Table 1). Both the whole-rock F and P_2O_5 contents increase with weak fluctuations from the first to fourth units, and increase strongly in the fifth unit (on average, 0.27 wt% → 0.35% → 0.44% → 0.43% →

1.66% F and 0.12 wt% → 0.12% → 0.20% → 0.27% → 0.56% P_2O_5) (Y1 to Y5, respectively, Table 1). On the basis of these criteria, the Yichun granite complex may be considered as an example of an amblygonite-type granite of Raimbault *et al.* (1991) or as a high-P subtype of F-rich granites as proposed by Taylor (1992).

In the topaz–lepidolite granite, the whole-rock SiO_2 contents decrease from the lower part to the middle part, and increases in the upper part. On the other hand, the whole-rock Al_2O_3, Na_2O, P_2O_5, and F contents increase from the lower part to the middle part, and decrease in the upper part (Table 1).
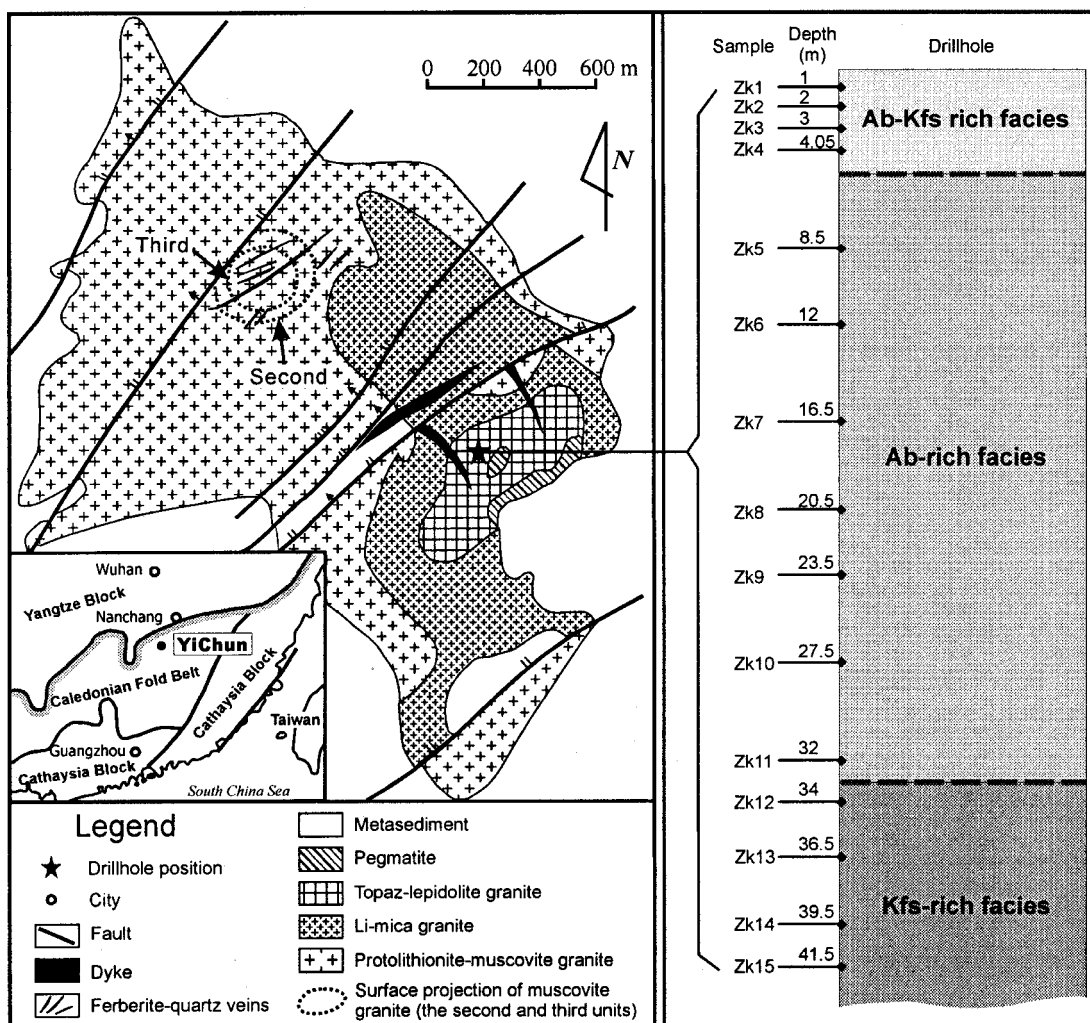

FIG. 1. Simplified geological map (after Yin *et al.* 1995) and cross-section of the Yichun topaz–lepidolite granite, drawn on the basis of drill-hole data.

The trace elements, including the rare-earth elements

The variations in trace-element concentrations in the Yichun granite complex are complicated. The contents of rare alkalis, such as Li and Rb, vary weakly in the three early stages, but are strongly enriched to 5296 ppm and 3269 ppm, respectively, in the later two stages (Table 1), in which lepidolite or Li-mica is abundant. High field-strength elements, such as Nb and Ta, increase weakly from the first stage to the fourth stage, and are enriched to 68.9 ppm and 137 ppm, respectively, in the fifth stage (Table 1). Disseminated tantalite, microlite, wodginite and Ta-rich cassiterite are relatively abundant in the topaz–lepidolite granite (Belkasmi *et al.* 2000, and see below), as is hafnian zircon.

The content of rare-earth elements (*REE*) of the Yichun granite complex is very low, and generally decreases from the early to late stages. The third stage, medium-grained muscovite granite, contains the highest Σ*REE*, 53.8 ppm (Table 1), that of the fifth stage is lowest. The average concentration reported by Yin *et al.* (1995) is 5 ppm, whereas the results of ICP–MS analyses of drill-hole samples are all less than 1.1 ppm (Table 1). The sum of the *REE* is variable in the drilled section also; it decreases from the lower part to the middle part, then increases in the upper part (Table 1).

TABLE 1. WHOLE-ROCK COMPOSITION OF THE YICHUN GRANITIC COMPLEX, CHINA

units	1	2	3	4	5						
Sample Number	Y1 3	Y2 3	Y3 3	Y4 3	Y5 4	Zk2 1	Zk3 1	Zk5 1	Zk9 1	Zk12 1	Zk13 1
SiO_2 wt%	75.12	74.73	74.47	74.00	68.12	71.43	67.92	69.32	68.91	74.67	74.49
TiO_2	0.10	0.05	0.08	0.05	0.04	0.00	0.00	0.01	0.01	0.01	0.00
Al_2O_3	14.04	14.00	13.61	15.39	18.45	16.18	18.88	17.30	17.53	14.83	15.33
TFeO						0.17	0.17	0.15	0.12	0.20	0.14
Fe_2O_3	0.40	0.37	0.47	0.11	0.15						
FeO	0.95	0.96	1.15	0.39	0.22						
MnO	0.12	0.31	0.13	0.16	0.12	0.19	0.13	0.14	0.11	0.16	0.12
MgO	0.22	0.15	0.27	0.03	0.02	0.18	0.08	0.00	0.08	0.18	0.08
CaO	0.46	0.36	0.39	0.16	0.09	0.14	0.14	0.08	0.18	0.44	0.14
Na_2O	3.48	3.66	3.13	4.80	6.35	4.14	6.23	5.01	6.56	3.02	4.31
K_2O	4.32	4.13	4.43	3.91	2.45	3.98	2.82	3.28	2.62	3.27	2.82
P_2O_5	0.12	0.12	0.20	0.27	0.56	0.33	0.23	0.55	0.40	0.49	0.15
Li_2O	0.11	0.05	0.08	0.14	1.14						
F	0.27	0.35	0.44	0.43	1.66	1.34	1.07	2.04	1.66	2.04	1.53
LOI						2.05	2.13	2.12	1.59	1.06	0.78
2F=O	-0.11	-0.15	-0.18	-0.18	-0.70	-0.56	-0.45	-0.86	-0.70	-0.86	-0.64
Total	99.50	99.07	98.67	99.66	98.64	99.57	99.35	99.14	99.07	99.51	99.25
A/NKC	1.25	1.26	1.28	1.24	1.40	1.43	1.40	1.45	1.26	1.60	1.48
Li ppm	511	232	372	650	5296	6569	6781	12059	10801	4579	3037
Rb	891	827	754	1786	3269	4589	3072	6423	4656	4180	2996
Sr	26.5	16	18.1	11	6.9	30.0	26.8	19.4	23.2	96.1	22.2
Zr	46.4	30.7	37.1	23.3	18.7	20.2	26.3	25.3	22.7	29.1	28.9
Nb	43	47	40	62	68.9	41.3	61.7	50.1	90.2	29.3	20.1
Cs	102.7			109.5	360	475	348	1709	743	328	220
Be						147	358	40	246	727	269
Ba						57.9	46.4	50.4	74.1	46.2	56.2
Hf						3.78	5.87	3.58	4.35	4.25	4.11
Ta	23.5	16.4	22	65	137	13.2	172.5	62	100.4	108.2	12.9
Th						2.46	3.36	2.41	2.12	3.47	2.91
Y	2.96	n.d.	n.d.	1.41	1.47	0.464	0.358	0.233	0.442	0.862	0.598
La	7.05	4.57	10.23	1.13	1.37	0.080	0.057	0.072	0.104	0.104	0.111
Ce	15.78	8.71	21.86	2.54	1.61	0.151	0.146	0.223	0.146	0.297	0.207
Pr	2.56	2.26	3.81			0.025	0.015	0.018	0.019	0.028	0.030
Nd	7.42	4.12	9.95	1.59	0.96	0.101	0.050	0.057	0.069	0.083	0.109
Sm	1.86	1.38	2.21	0.92	0.47	0.061	0.048	0.039	0.043	0.101	0.094
Eu	0.14	0.03	0.16	0.12	0.05	0.007	0.002	0.002	0.003	0.003	0.005
Gd	1.64	0.97	1.53	0.8	0.52	0.093	0.070	0.047	0.066	0.157	0.144
Tb	0.29	0.36	0.39			0.030	0.022	0.014	0.024	0.055	0.042
Dy	1.38	1.74	1.57			0.116	0.084	0.054	0.100	0.202	0.165
Ho	0.24	0.35	0.30			0.011	0.006	0.004	0.007	0.013	0.011
Er	0.66	0.79	0.65			0.025	0.013	0.010	0.012	0.019	0.018
Tm	0.15	0.20	0.16			0.003	0.002	0.001	0.002	0.002	0.002
Yb	0.76	1.49	0.88			0.024	0.011	0.008	0.012	0.010	0.011
Lu	0.14	0.18	0.11	0.03	0.03	0.004	0.002	0.001	0.001	0.002	0.002
Σ*REE*	40.07	27.15	53.81	7.13	5.01	0.731	0.528	0.550	0.584	1.076	0.951

Units: 1: medium- to coarse-grained protolithionite–muscovite granite; 2: fine-grained porphyritic muscovite granite; 3: medium-grained muscovite granite; 4: Li-mica granite; 5: topaz–lepidolite granite. Y1, Y2, Y3, Y4, and Y5 are average data from Yin *et al.* (1995); A/NKC: $Al_2O_3/(Na_2O + K_2O + 2CaO)$ (moles). TFeO: total iron expressed as FeO.

All the chondrite-normalized *REE* patterns of the Yichun granite complex are distinctly of V-shape, with strong depletion in Eu (Fig. 2). In the drilled section, Sm and Dy are both enriched, which is very much like the M-type of *REE* pattern of the Jiankengli leucogranite, in Jiangxi Province, China (Masuda *et al.* 1987). This pattern of enrichment results from the lanthanide tetrad effect, and the strong participation of aqueous complexes.

MINERALOGY

The Yichun topaz–lepidolite granite consists of quartz, the feldspars, topaz, and lepidolite, and contains accessory phosphates (amblygonite, "apatite", triplite, herderite, and xenotime), zircon, thorite, oxide minerals of Nb–Ta–Sn (columbite, microlite, wodginite, and cassiterite). The association of accessory minerals in the Yichun topaz–lepidolite granite is shown in Table 2.

THE FELDSPARS

The feldspars are demonstrated to be important phosphorus-bearing phases in P-rich granitic rocks (London 1992, Bea *et al.* 1994, Kontak *et al.* 1996, London *et al.* 1999). Albite and K-feldspar from the Yichun topaz–lepidolite granite were studied in detail with the electron microprobe.

K-feldspar

A microscope investigation reveals that K-feldspar is most abundant in the lower part of the topaz–lepidolite granite, and rare in the middle part, where albite becomes the dominant feldspar phase. Two generations of K-feldspar may be clearly recognized. The early generation occurs as phenocrysts containing fine tabular albite along growth zones (Fig. 3a), which is generally named the "snowball" texture (Yin *et al.* 1995). However, in the middle part, the K-feldspar phenocrysts were almost completely transformed into muscovite and quartz, whereas the fine tabular albite inclusion was preserved within the pseudomorphs after the K-feldspar phenocrysts. The K-feldspar of the late generation consists of fine-grained anhedral crystals. Unlike some grains of K-feldspar from P-high granites (Kontak *et al.* 1996), the K-feldspar of the Yichun granite all seems nonperthitic. Electron-microprobe analyses of K-feldspar show the homogeneous development of the end-member composition ($Or_{98–99}Ab_{2–1}$) in both fine-grained anhedral crystals and phenocrysts, but great variability in P_2O_5 contents (Tables 3, 4). For example, in the sample Zk12, the early K-feldspar contains relatively low phosphorus (0.23 wt% P_2O_5, Table 3), whereas the P content of the late generation is much higher (up to 0.79 wt% P_2O_5, Table 3). This pattern could be attributed to an increase in P with magmatic evolution.

Albite

Three generations of albite are distinguished in the granite. The first generation consists of sub- to euhedral, tabular phenocrysts (~0.5 mm wide, ~0.8 mm long; Fig. 3c). The second generation consists of albite inclusions that occur as fine tabular crystals occupying the growth zones within K-feldspar or quartz phenocrysts (the "snowball" texture: Figs. 3a, b). The third generation of albite consists of fine tabular crystals in the groundmass of the granite (0.03–0.2 mm wide, 0.2–0.5 mm long: Fig. 3c).

TABLE 2. SUMMARY OF DISTRIBUTION OF ACCESSORY MINERALS IN THE YICHUN TOPAZ–LEPIDOLITE GRANITE, CHINA

Facies	Depth	Phosphate minerals					Nb–Ta oxide minerals					
Sample	(m)	Amb	Fap	Xnt	Tph	Hrd	Zrn	Thr	Cbt	Wdg	Mic	Cst
III Zk1	1		+++	+	+		++	+	+++			+
Zk2	2						++		++	+		+
Zk3	3						++		++	+		
Zk4	4.05						+		+			+
II Zk5	8.5	+++					++	+	+++		+++	
Zk6	12	+++				+	+		++		++	+
Zk7	16.5	++	+			+	++		+++		+++	++
Zk8	20.5	+					++	+	+++	+	+	+
Zk9	23.5	+++	++				++		+++			++
Zk10	27.5	+++	++				++	+	+++			+
Zk11	32						++		+			+
I Zk12	34		+			++	++		+	+++		++
Zk13	36.5						+		+	+		+
Zk14	39.5						++		+	+	+	+
Zk15	41.5						++		+			+

Symbols: Amb: amblygonite, Fap: apatite, Xnt: xenotime, Tph: triplite, Hrd: herderite, Zrn: zircon, Thr: thorite, Cbt: columbite-group minerals (columbite and tantalite), Wdg: wodginite-group minerals, Mic: microlite, Cst: cassiterite. +++: abundant, ++: present, +: rare. I: Kfs-rich facies, II: Albite-rich facies, III: Albite–Kfs-rich facies.
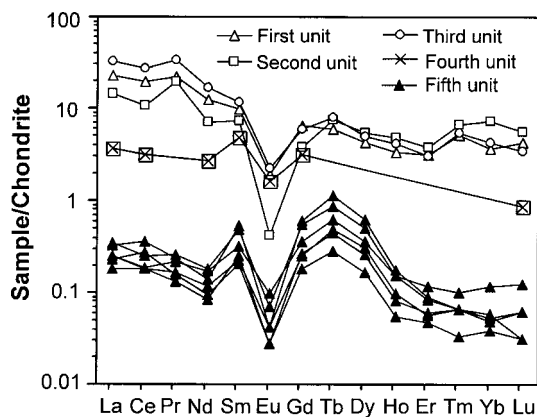

FIG. 2. Chondrite-normalized *REE* patterns of the Yichun granite complex (data for the first four units from Yin *et al.* 1995).
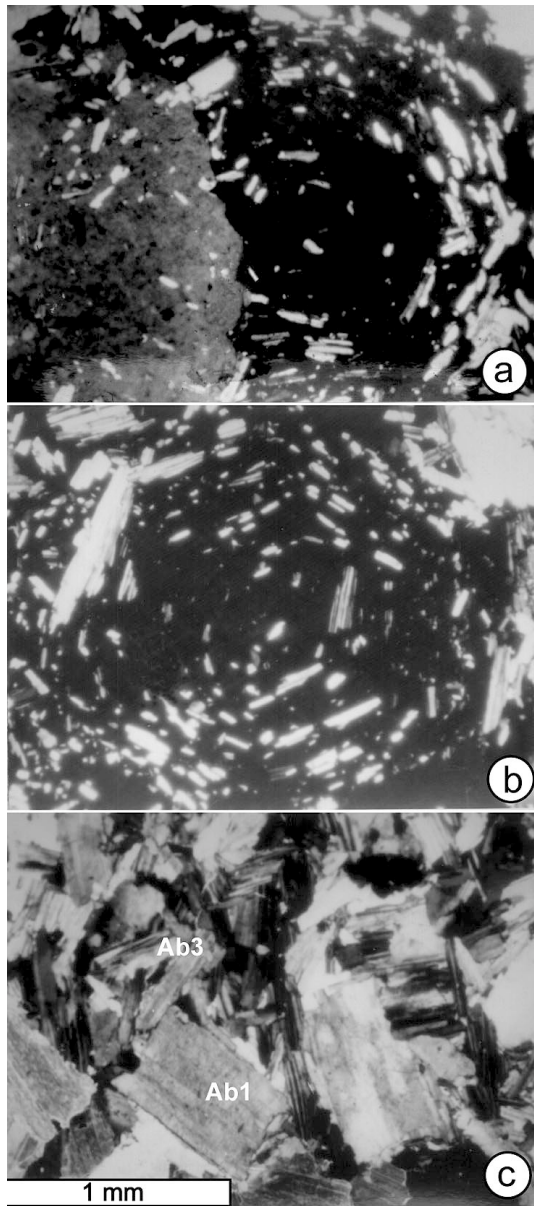
FIG. 3.   Microphotographs of the feldspars (crossed-polarized light). The "snowball" texture: fine-tabular crystals of albite (white) occupying growth zones within K-feldspar phenocrysts (a) and quartz phenocrysts (b). (c) Tabular phenocrysts of first-generation albite (Ab1) and fine-tabular crystals of third-generation albite (Ab3).

Like the K-feldspar, the albite is chemically homogeneous ($Ab_{98}Or_1An_1$), but variable in phosphorus content. The early generation of albite contains a lower level of phosphorus than the later generation (Table 3), such that the P_2O_5 content of the albite groundmass (*i.e.*, 0.93 wt% in sample Zk2) is distinctly higher than that of the adjacent early-generation albite phenocrysts (0.35 wt% in sample Zk2). The distribution of phosphorus in the different generations of albite indicates that the magma was initially relatively poor in phosphorus, but became enriched during magmatic evolution. The P_2O_5 content is also variable in single crystals of albite, especially where secondary inclusions of apatite are enclosed (see below for more detail).

Distribution of phosphorus between the feldspars

Many studies have demonstrated that phosphorus is significant in both K-feldspar and albite, but the distribution of phosphorus between feldspars is complicated. London (1992) and Kontak *et al.* (1996) have shown that phosphorus prefers to enter the structure of K-feldspar relative to that of albite. However, London *et al.* (1999) revealed some cases of a distribution coefficient ($D_P^{Kfs/Pl}$) lower than unity.

In the Yichun topaz–lepidolite granite, the P content of albite is generally higher than that of K-feldspar in the same sample. The calculated distribution-coefficient $D_P^{Kfs/Pl}$ values of the samples are almost all lower than unity except for sample Zk1, with $D_P^{Kfs/Pl}$ value of 2.17 (Table 4). Compared to the adjacent albite, a K-feldspar typically contains a remarkably lower level of P. As an example, in sample Zk3 from the upper part of the drill hole, a K-feldspar crystal contains up to 0.10 wt% P_2O_5 (0.03 wt% on average, $n = 6$), whereas the adjacent albite contains between 0.06 and 0.48 wt% P_2O_5 (0.29 wt% on average, $n = 9$). Furthermore, the value of $D_P^{Kfs/Pl}$ displays a decreasing trend from the lower part to the middle part of the unit, but increases at the top (Table 4). London *et al.* (1993) determined a distribution coefficient ($D_P^{Kfs/Pl}$) of *ca.* 1.2 between coexisting Kfs and Pl in equilibrium, and deviations from this value reflect a lack of equilibrium between the Kfs–Pl pairs (London *et al.* 1999). Whereas albite and K-feldspar of the Yichun topaz–lepidolite granite are all pure phases, the various distribution coefficients, which markedly deviate from ~1.2, must also indicate a lack of equilibrium between albite and K-feldspar.

In the case of the "snowball" texture (Fig. 4), the P content of the early-generation K-feldspar is up to 0.40 wt%, and mostly lower than 0.10 wt% P_2O_5, with an average of 0.06 wt%, whereas the albite inclusions have a higher P content, mostly above 0.10 wt% P_2O_5. From core to rim of the "snowball", the P content of the host K-feldspar varies irregularly, whereas that of the albite inclusions has an increasing trend (Fig. 4), which implies that K-feldspar must have re-equilibrated at

TABLE 3. REPRESENTATIVE EMPA RESULTS OF FELDSPAR MINERALS
FROM THE YICHUN TOPAZ–LEPIDOLITE GRANITE, CHINA

| Generations	Zk1				Zk2			Zk7			Zk12	
	Ab First	Ab Third	Kfs Early	Kfs Late	Ab First	Ab Second	Ab Third	Ab First	Ab Second	Ab Third	Kfs Early	Kfs Late
SiO_2 wt%	67.48	67.38	64.54	64.22	68.47	67.96	67.00	68.82	67.95	67.09	64.49	63.23
Al_2O_3	19.82	20.49	18.91	19.50	20.29	19.86	19.97	20.47	19.75	20.53	19.42	19.43
P_2O_5	0.16	0.21	0.18	0.30	0.35	0.38	0.93	0.17	0.24	0.40	0.23	0.79
Na_2O	11.74	11.11	0.18	0.19	11.21	11.41	11.78	11.09	11.99	10.81	0.15	0.12
K_2O	0.03	0.16	15.66	15.98	0.15	0.14	0.11	0.07	0.11	0.20	15.15	15.89
CaO	b.d.l.	0.09	b.d.l.	b.d.l.	0.22	0.13	0.20	0.07	0.04	0.09	b.d.l.	b.d.l.
BaO	0.08	b.d.l.	0.17	b.d.l.	b.d.l.	b.d.l.	0.04	b.d.l.	b.d.l.	b.d.l.	b.d.l.	0.02
Total	99.30	99.43	99.63	100.17	100.68	99.87	100.02	100.70	100.07	99.11	99.44	99.47
Si *apfu*	2.970	2.955	2.983	2.954	2.965	2.969	2.929	2.975	2.970	2.949	2.972	2.928
Al	1.028	1.059	1.030	1.057	1.035	1.023	1.029	1.043	1.017	1.063	1.054	1.060
P	0.006	0.008	0.007	0.012	0.013	0.014	0.034	0.006	0.009	0.015	0.009	0.031
Na	1.002	0.945	0.016	0.017	0.941	0.966	0.999	0.929	1.016	0.921	0.013	0.011
K	0.002	0.009	0.924	0.938	0.008	0.008	0.006	0.004	0.006	0.011	0.890	0.939
Ca		0.004			0.010	0.006	0.009	0.003	0.002	0.004		
Ba	0.001		0.003				0.001					0.000
Or mol.%	0.2	0.9	98.3	98.2	0.8	0.8	0.6	0.4	0.6	1.2	98.6	98.8
Ab	99.8	98.6	1.7	1.8	98.1	98.6	98.5	99.3	99.2	98.4	1.4	1.2
An	0.0	0.4	0.0	0.0	1.0	0.6	0.9	0.3	0.2	0.4	0.0	0.0
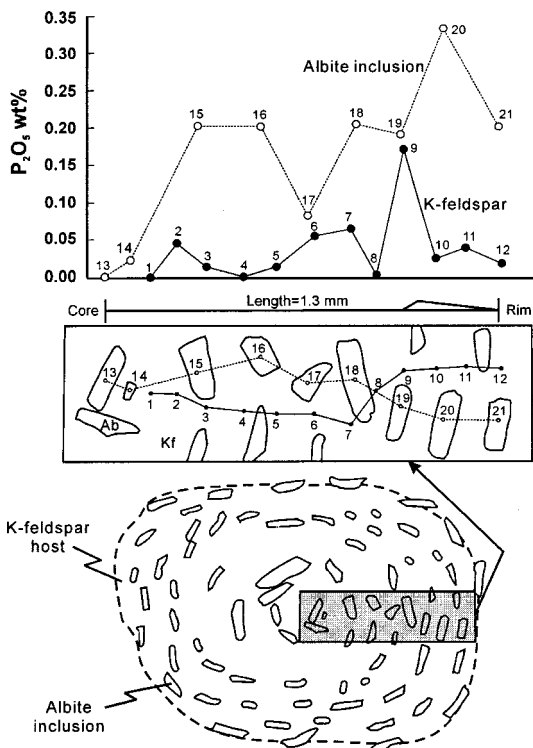
FIG. 4. Variations in P_2O_5 contents in the host K-feldspar phenocryst and the albite inclusions in the "snowball".

TABLE 4. PHOSPHORUS CONTENT IN FELDSPARS IN
THE YICHUN TOPAZ–LEPIDOLITE GRANITE, CHINA

Facies	Sample	albite (Ab)		K-feldspar (Kfs)		$D_P^{Kfs/Pl}$
		average	min. / max.	average	min. / max.	
III	Zk1	0.10 (19)	b.d.l. / 0.21	0.22 (15)	0.07 / 0.40	2.17
	Zk2	0.48 (7)	0.28 / 0.93	0.15 (2)	0.10 / 0.20	0.32
	Zk3	0.23 (45)	b.d.l. / 0.48	0.03 (37)	b.d.l. / 0.17	0.14
	Zk4	0.24 (8)	0.17 / 0.32			
II	Zk5	0.26 (8)	0.23 / 0.29	0.02 (6)	b.d.l. / 0.05	0.07
	Zk6	0.29 (11)	0.14 / 0.50	0.04 (3)	0.03 / 0.06	0.14
	Zk7	0.22 (25)	b.d.l. / 0.51	0.03 (17)	b.d.l. / 0.08	0.14
	Zk8	0.16 (9)	0.06 / 0.28	0.03 (4)	0.02 / 0.04	0.20
	Zk9	0.23 (6)	0.15 / 0.32			
	Zk10	0.18 (5)	0.10 / 0.26			
	Zk11	0.18 (10)	b.d.l. / 0.30			
I	Zk12	0.49 (6)	0.31 / 0.82	0.39 (8)	0.07 / 0.79	0.79
	Zk13	0.23 (5)	0.19 / 0.29	0.21 (2)	0.16 / 0.25	0.88
	Zk14	0.27 (4)	0.11 / 0.40	0.16 (1)		0.59
	Zk15	0.20 (5)	0.14 / 0.30	0.08 (5)	0.02 / 0.18	0.41

Facies: I: Kfs-rich facies, II: Ab-rich facies, III: Ab–Kfs-rich facies. b.d.l. = below the detection limits. The phosphorus content is expressed as the oxide, P_2O_5 (wt%).

subsolidus conditions, whereas the albite inclusions are still pristine.

Cases where $D_P^{Kfs/Pl}$ is much lower than 1 are mostly interpreted by invoking crystallization of plagioclase before K-feldspar or by recrystallization of K-feldspar after depletion of P in the melt (London 1992). However, the first hypothesis seems unlikely to be suitable for the Yichun topaz–lepidolite granite. The petrographic characteristics, such as "snowball"-textured K-feldspar phenocrysts with albite inclusions, and albite groundmass, suggest that the K-feldspar crystallized

before, or at least contemporary with, the albite. The secondary apatite (see below for a detailed discussion) and the pure end-member composition of K-feldspar all imply that K-feldspar must have completely re-equilibrated at a low temperature.

LI-RICH MICA

In the Yichun topaz–lepidolite granite, the mica usually occurs as fine tabular crystals in the groundmass, and is represented by Li-rich members, whose composition, like that of the feldspar, differs depending on the petrographic facies. In the lower part of the granite, mica corresponds to Fe-bearing lepidolite (1.44 wt% FeO, sample Zk15). Nearly pure lepidolite is observed in the middle part, where FeO is generally below 0.20 wt%. The occurrence of zinnwaldite instead of lepidolite is noteworthy in the near-surface sample of the upper part (up to 7.39 wt% FeO in sample Zk1). Representative electron-microprobe analyses allowed us to calculate the structural formulae of the micas based on 11 atoms of oxygen and assuming stoichiometry: upper facies, Zk1: $(K_{0.909}Na_{0.029})(Al_{1.309}Li_{0.982}Fe^{2+}_{0.392}Mn_{0.051})[(Si_{3.414}$ $Al_{0.586})O_{10}](F_{1.556}OH_{0.444})$, middle facies, Zk6: $(K_{0.884}$ $Na_{0.024}Cs_{0.013}Rb_{0.005})(Al_{1.287}Li_{1.459}Fe^{2+}_{0.002}Mn_{0.003})$ $(Si_{3.615}Al_{0.385})O_{10}](F_{1.786}H_{0.214})$, lower facies, Zk15: $(K_{0.908}Na_{0.053})(Al_{1.342}Li_{1.155}Fe^{2+}_{0.074}Mn_{0.052})[(Si_{3.464}$ $Al_{0.536})O_{10}](F_{1.647}\,OH_{0.353})$. It is interesting to note that lepidolite in the middle part is commonly rimmed by Cs-rich mica (up to 22.71 wt% Cs_2O, detailed study in progress). The occurrence of a cesian lepidolite rim

implies the presence of a Cs-rich late-magmatic fluid, which reflect the very high Cs content of whole rock, *i.e.*, 1709 ppm in sample Zk5 (Table 1).

TOPAZ

Topaz is present in the Yichun topaz–lepidolite granite. Euhedral to subhedral phenocrysts enclose magmatic accessory minerals such as columbite and zircon, and may be considered as one of the early phases of crystallization. Electron-microprobe results show that in all cases, the topaz is fluorine-dominated in the anion site (17.43 < F < 18.78 wt%), also suggestive of a magmatic origin for this mineral (Rosenberg 1972).

THE PHOSPHATES

In the Yichun topaz–lepidolite granite, both "monazite" and "xenotime" are rarely observed, whereas "apatite" and amblygonite are essential phosphate minerals, but in low modal proportion. "Apatite" is present in all facies, and amblygonite occurs only in the middle part of the drilled section (Table 2).

Apatite-group phase

"Apatite" is observed mainly in the middle and upper facies, but only sporadically in the lower facies. On the basis of back-scattered electron images, three types of "apatite" are recognized: (1) anhedral "apatite" fills the interstices among the grains of feldspar, quartz and lepidolite, mainly in the middle and upper parts of the drilled section; (2) euhedral inclusions (~80 μm) in albite in the upper part of the drill hole, and (3) fine-grained (~10 μm), anhedral grains of secondary origin distributed along the cleavages of feldspar. This type is infrequently observed in all facies.

Electron-microprobe results indicate that the apatite-group mineral is fluorapatite, but it shows major compositional variations, particularly in Mn content. The anhedral fluorapatite (type 1) contains elevated contents of Mn (up to 4.29 wt% MnO, Table 5). Inclusions of euhedral fluorapatite enclosed in albite are also enriched in Mn, and generally are compositionally zoned, with a slight core-to-rim decrease in Mn (nos. 3–5, Table 5). These euhedral crystals are products of early-stage crystallization. In contrast, the inclusions of fluorapatite are relatively poor in Mn (Table 5). Note that the P content of the host feldspar has dropped sharply at its contact with the apatite (Zk10, Table 6). This pattern suggests a release of P from the feldspar structure as it undergoes Al–Si ordering in the presence of the fluid medium carrying Ca, leading to *in situ* formation of an apatite-group mineral (Kontak *et al.* 1996). Therefore, this type of "apatite", present as inclusions, seems to be of secondary origin.

TABLE 5. REPRESENTATIVE COMPOSITION OF FLUORAPATITE FROM THE YICHUN TOPAZ–LEPIDOLITE GRANITE, CHINA

	1	2	3	4	5	6	7	8	9
P_2O_5 wt%	39.90	40.91	39.99	39.53	40.60	42.61	41.84	42.44	41.79
CaO	50.27	51.73	50.09	51.50	51.67	52.02	53.63	52.19	53.66
FeO	0.03	0.02	0.04	b.d.l.	0.02	b.d.l.	0.02	0.02	b.d.l.
MnO	4.29	2.02	3.82	3.61	3.02	2.50	0.29	2.45	0.21
Al_2O_3	b.d.l.	0.09	b.d.l.	b.d.l.	0.04	0.02	0.01	0.02	0.01
SiO_2	0.01	0.23		0.03	0.15	0.04	0.01	0.04	0.04
Na_2O	0.06	0.05	0.04	0.07	0.15	0.05	b.d.l.	0.01	0.01
SrO	0.22	0.22	0.18	0.19	0.25	0.01	b.d.l.	b.d.l.	b.d.l.
F	3.57	3.30	3.34	3.14	2.43	2.81	2.97	3.12	3.48
Cl	b.d.l.	b.d.l.	b.d.l.	0.02	b.d.l.	b.d.l.	b.d.l.	0.01	b.d.l.
2F,2Cl=O	-1.50	-1.39	-1.40	-1.32	-1.02	-1.18	-1.25	-1.31	-1.46
Total	96.85	97.19	96.10	96.74	97.31	98.88	97.52	98.95	97.70
P *apfu*	2.970	2.995	2.986	2.943	2.973	3.043	3.026	3.037	3.025
Ca	4.736	4.794	4.733	4.852	4.788	4.701	4.909	4.726	4.913
Fe	0.002	0.001	0.003		0.001		0.001	0.001	
Mn	0.320	0.148	0.286	0.269	0.221	0.179	0.021	0.175	0.015
Al		0.009			0.004	0.002	0.001	0.002	0.001
Si	0.001	0.020		0.003	0.013	0.003	0.001	0.001	0.003
Na	0.010	0.008	0.007	0.012	0.025	0.008		0.002	0.002
Sr	0.011	0.011	0.009	0.010	0.013	0.000			
F	0.993	0.902	0.932	0.872	0.665	0.748	0.801	0.834	0.940
Cl				0.003				0.001	

b.d.l.: below detection limits. The structural formulae are calculated on the basis of twelve atoms of oxygen; *apfu*: atoms per formula unit. Columns 1–5: Zk1. 1: anhedral grain, interstitial between Ab and Kfs. 2: secondary fluorapatite, in Ab. 3–5: euhedral inclusion in Ab, composition of the core (3), subrim (4) and rim (5). Columns 6 and 7: Zk9. 6: anhedral grain, interstitial among Ab grains. 7: secondary fluorapatite, in Ab. Columns 8 and 9: Zk10. 8: anhedral grain, interstitial between Ab and Kfs. 9: secondary fluorapatite, in Ab.

Amblygonite group

Although the concentration of lithium cannot be determined by electron microprobe, amblygonite was easily recognized in the middle part of the section. It occurs notably as anhedral crystals interstitial with respect to feldspars and lepidolite (Figs. 5a, b), and is also characterized by turbidity due to micro-inclusions. The composition of the amblygonite at Yichun is nearly constant (Table 7), with an analytical total generally below 90 wt%.

The phosphorus content of albite adjacent to the amblygonite is distinctively higher than average, and there is a Ca-poor, P-rich filling along the cleavages in albite (Figs. 5c,d).

Triplite

Triplite is only observed as interstitial anhedral grains in the upper part of the drilled section. Representative electron-microprobe results on triplite are listed in Table 7, and the calculated structural formula based on four atoms of oxygen is $(Mn_{1.779}Fe_{0.131}Ca_{0.098})_{\Sigma 2.008}$ $[(P_{0.993}Si_{0.005})_{\Sigma 0.998}O_4](F, OH)$.

Other phosphates

"Monazite" and "xenotime" are both widespread accessory minerals in granites or granitic pegmatites. The former is the main reservoir of the light rare-earth elements (*LREE*), Th, and U in peraluminous granites, whereas the latter is an important reservoir of Y and the heavy rare-earth elements (*HREE*) (Wark & Miller 1993, Hinton & Paterson 1994, Bea *et al.* 1994, Bea 1996, Förster *et al.* 1998a, b). But they are rarely found in the Yichun topaz–lepidolite granite, and mainly occur at the early stage of crystallization in the complex. The "xenotime" observed in the drill core occurs as very fine-grained (<10 μm) anhedral crystals.

Other phosphate minerals have been identified. In the middle and lower parts of the section, we have identified herderite on the basis of electron-microprobe data (Table 2); it is similar to the herderite in the Beauvoir granite, France (Charoy 1999; Table 8). The presence of very high levels of beryllium in the Yichun topaz–lepidolite granite (up to 727 ppm, Zk12: Table 1) indicates the possibility of the existence of beryllium-bear-

TABLE 6. COMPOSITIONAL VARIATION OF ALBITE CONTAINING SECONDARY APATITE, YICHUN TOPAZ–LEPIDOLITE GRANITE, CHINA

Point No.	Albite A				Albite B			
	A1	A2	A3	A4	B1	B2	B3	B4
SiO_2 wt%	68.94	67.69	67.90	68.99	67.81	68.75	68.69	68.55
Al_2O_3	19.30	19.10	19.88	19.20	19.11	19.07	19.69	19.59
Na_2O	11.42	11.36	11.38	11.60	11.69	10.75	11.11	11.39
K_2O	0.06	0.14	0.07	0.07	0.03	0.13	0.10	0.12
CaO	0.06	0.04	0.11	0.08	0.07	b.d.l.	0.02	0.09
P_2O_5	0.01	0.05	0.25	0.11	0.02	0.08	0.11	0.26
BaO	b.d.l.	0.12	b.d.l.	0.39	0.20	0.22	b.d.l.	b.d.l.
Total	99.79	98.50	99.59	100.44	98.93	99.00	99.72	100.00
Si *apfu*	3.01	3.00	2.97	3.01	3.00	3.02	3.00	2.99
Al	0.99	1.00	1.03	0.99	1.00	0.99	1.01	1.01
Na	0.97	0.98	0.97	0.98	1.00	0.92	0.94	0.96
K	0.00	0.00	0.00	0.00	0.00	0.00	0.00	0.00
Ca	0.00	0.00	0.01	0.00	0.00		0.00	0.00
P	0.00	0.00	0.01	0.00	0.00	0.00	0.00	0.01
Ba		0.00		0.01	0.00	0.00		
Total	4.98	4.99	4.98	4.99	5.00	4.94	4.96	4.98
Ab mol.%	99.62	99.60	99.37	99.52	99.63	99.80	99.75	99.39
Or	0.09	0.20	0.10	0.10	0.04	0.20	0.15	0.17
An	0.29	0.19	0.53	0.38	0.33	0.00	0.10	0.43

The sequences A1 to A4 and B1 to B4 indicate distance away from the secondary apatite in two host crystals of albite in sample Zk-10, respectively. b.d.l.: below detection limits. The structural formulae are calculated on the basis of eight atoms of oxygen.

TABLE 7. PARTIAL COMPOSITIONS OF AMBLYGONITE AND TRIPLITE FROM THE YICHUN TOPAZ–LEPIDOLITE GRANITE, CHINA

	Amblygonite						Triplite	
	Zk5 1	Zk6 2	Zk7 3	Zk8 4	Zk9 5	Zk10 6	Zk1	Zk1
P_2O_5 wt%	50.40	51.69	51.93	51.27	51.25	47.94	31.29	31.29
CaO	0.03	0.07	0.01	0.05	0.02	0.02	2.32	2.45
FeO	b.d.l.	b.d.l.	b.d.l.	b.d.l.	b.d.l.	b.d.l.	4.39	4.16
MnO	b.d.l.	b.d.l.	0.01	b.d.l.	0.04	0.04	55.98	56.02
Al_2O_3	35.97	35.54	36.88	35.36	36.35	35.47	0.04	0.00
SiO_2	0.06	0.06	0.05	0.02	0.24	0.42	0.07	0.14
Li_2O*	10.64	10.73	10.95	10.62	10.80	10.25		
F	6.29	4.54	4.27	4.66	7.53	7.79	n.d.	n.d.
2F=O	-3.64	-2.63	-2.48	-2.70	-4.37	-4.51		
Total	99.75	100.00	101.63	99.24	101.89	97.42	94.08	94.06
P *apfu*	1.001	1.015	1.003	1.015	1.001	0.984	0.993	0.993
Ca	0.001	0.002	0.000	0.000	0.001	0.001	0.093	0.098
Fe							0.138	0.131
Mn			0.000		0.001	0.001	1.779	1.779
Al	0.995	0.972	0.992	0.974	0.989	1.013	0.002	0.000
Si	0.001	0.001	0.001	0.001	0.006	0.010	0.003	0.005
Li*	1.004	1.001	1.005	0.999	1.002	0.999		
F	0.467	0.333	0.308	0.345	0.550	0.597		

* The amounts of Li_2O and Li are calculated by stoichiometry. b.d.l.: below detection limits; n.d.: not detected. The structural formulae are calculated on the basis of four atoms of oxygen. *apfu*: atoms per formula unit.

TABLE 8. PARTIAL COMPOSITION OF HERDERITE FROM THE YICHUN TOPAZ–LEPIDOLITE GRANITE, CHINA

	Yichun granite (Zk6)					Beauvoir granite		Theoretical compositions	
	1	2	3	4	5	B.5	B.2	Hrd	Hhrd
P_2O_5	44.61	42.98	42.52	42.35	41.64	43.63	42.39	43.52	44.06
CaO	33.34	32.17	32.50	32.58	32.30	34.65	31.58	34.39	34.82
FeO	b.d.l.	b.d.l.	b.d.l.	b.d.l.	0.11				
MnO	0.02	0.01	0.09	b.d.l.	0.03				
Al_2O_3	b.d.l.	0.02	b.d.l.	b.d.l.	b.d.l.				
SiO_2	0.10	0.28	0.17	0.07	0.25				
F	5.31	7.03	5.91	7.28	5.19	4.05	4.18	11.65	
2F=O	-2.23	-2.95	-2.48	-3.06	-2.18	-1.70	-1.76	-4.89	
BeO*	15.76	15.27	15.05	14.96	14.78	15.63	16.74	15.33	15.53
H_2O*	5.01	3.55	4.35	3.24	4.84	3.60	3.75		5.59
Total	101.92	98.36	98.11	97.42	96.94	99.86	96.88	100.00	100.00

*: The amounts of BeO and H_2O are calculated by stoichiometry. Samples 5 and 2 from the Beauvoir granite are from Charoy (1999). b.d.l.: below detection limits. The compositions are reported in wt%. Symbols: Hrd: herderite, Hhrd: hydroxylherderite.
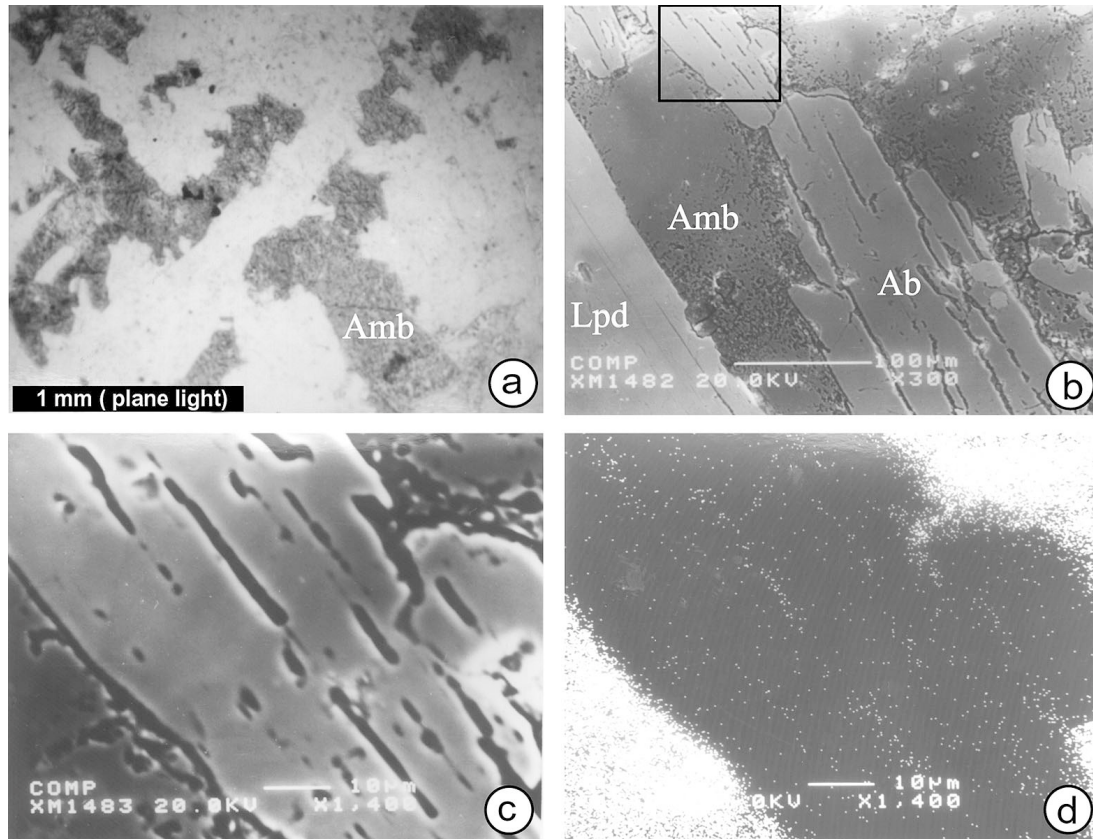
FIG. 5. (a) Amblygonite (Amb) interstitial to feldspars or lepidolite. Plane-polarized light. (b) Back-scattered-electron image of amblygonite (Amb) filling the interspace between albite (Ab) and lepidolite (Lpd). (c) Enlargement of (b). (d) Phosphorus X-ray scan image of (c), showing the relatively higher phosphorus content in a cleavage and at the rim of the albite relative to the body of the albite.

ing minerals such as herderite. Herderite is considered as a secondary mineral in rare-metal-bearing granites, and crystallizes at relatively low temperatures (~250°C) (Charoy 1999). Thus, herderite may be the result of postmagmatic alteration.

In addition, qualitative analysis shows an unknown P, Sn, and Bi-bearing phase along cleavage of albite and K-feldspar from the middle and lower parts of the section. As in the case of herderite, this P-bearing phase results from postmagmatic alteration.

ZIRCON

Zircon is an accessory mineral present throughout the Yichun granite. It occurs as subhedral to euhedral crystals from 2 to 100 μm across, with well-developed tetragonal dipyramids. It is usually enclosed in lepidolite or topaz, but becomes interstitial between quartz and feldspars in the upper part of the section, as observed in other rare-element granites (*e.g.,* Wang *et al.* 1992, 1996). The zircon is commonly zoned, with one type characterized by a progressive increase in brightness (BSE imaging) from the core to the rim of crystals (Fig. 6a). Another pattern of zonation is shown by a porous core and relatively intact rim (Fig. 6b). Striking differences in composition (*e.g.,* Hf and U contents) are observed between the intact rim and the porous core, which suggests that the core represents a relic of the zircon, and the rim overgrows it during crystallization of the host granitic magma. Crystals of zircon without zoning are homogeneous in chemical composition, and are all euhedral. Zircon is generally intergrown with other accessory minerals such as columbite, cassiterite, thorite (Figs. 6c, d), and may contain small inclusions of thorite (Fig. 6d).

Fifty-nine analyses of twenty grains of zircon reveal a complex chemical composition (Table 9).
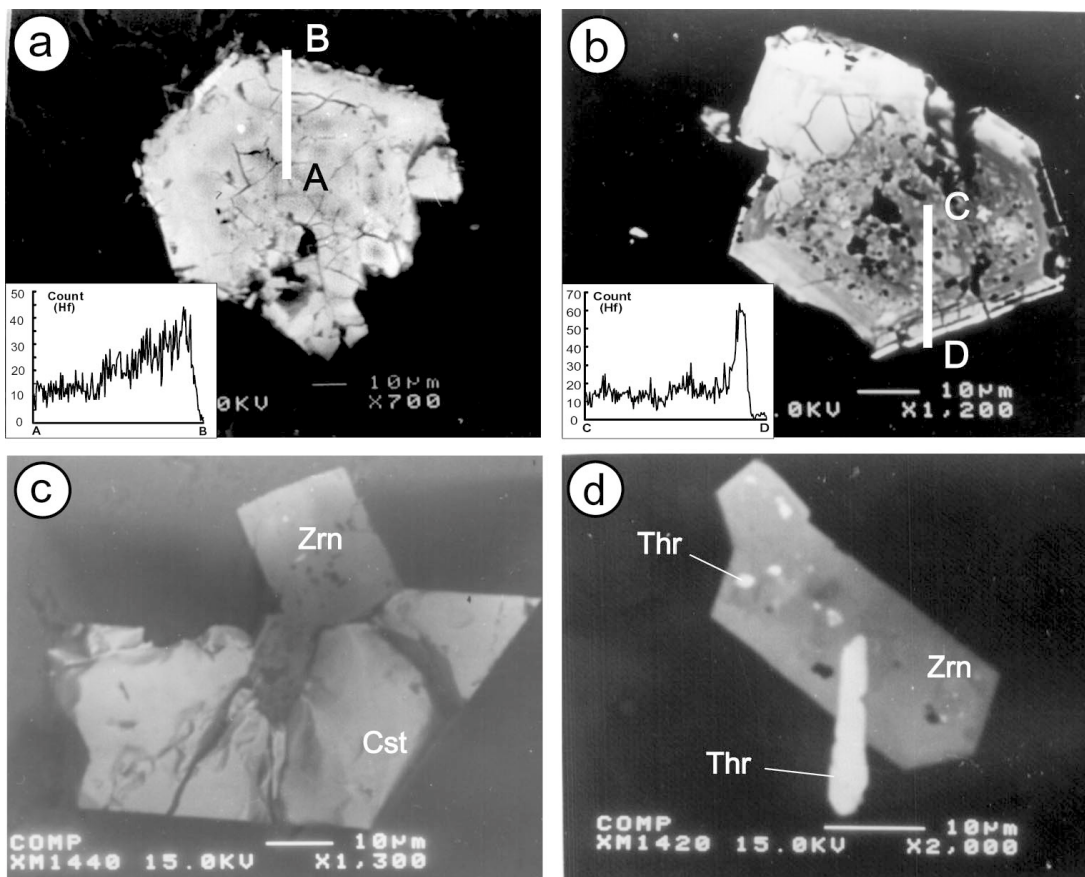
FIG. 6. Back-scattered-electron image of zircon. (a) Zoned zircon with a progressive increase in Hf content from core to rim. (b) Zircon with a porous relict core (low in Hf) and overgrown by a Hf-rich rim. (c) Zircon (Zrn) intergrown with cassiterite (Cst). (d) Zircon (Zrn) intergrown with thorite (Thr). Insets in (a) and (b) correspond to Hf counts along lines A–B and C–D, revealing an enrichment in Hf at the rim.

Hafnium

The hafnium content varies from 2.66 to 21.98 wt% HfO_2, but mostly from 4 to 8 wt% (Fig. 7a). According to the nomenclature proposed by Correia Neves *et al.* (1974), most of the compositions pertain to hafnian zircon, which is similar to zircon of other rare-element-enriched granites, such as the Beauvoir granite, Massif Central, France (Wang *et al.* 1992), the Suzhou granite, eastern China (Wang *et al.* 1996), and the Xihuashan granite, southern China (unpubl. data of Ru Cheng Wang). The Hf content of zircon is variable on both the single-crystal and drill-hole scales. First, a core-to-rim increase in Hf content is observed in single crystals. Where zoning is evident, the rim generally contains more Hf than the core (*e.g.,* sample Zk7: Fig. 6a). A traverse across a zoned crystal of zircon (sample Zk5)

reveals a sharp increase in Hf toward the rim (Fig. 6b). The relict core of this zircon contains 4.53 wt% HfO_2, whereas the rim contains up to 21.98 wt% HfO_2 (no. 2 and 3, Table 9). Second, the Hf content of zircon varies on the scale of the drill hole, and tends to increase from the lower part to the middle part, then to decrease upward (Fig. 8a).

Uranium and thorium

The Yichun zircon generally contains of 0.11 to 4 wt% UO_2 (Fig. 7b), in some cases reaching 9.94 wt% UO_2 (no.11, Table 9), a value very close to the theoretical maximum UO_2 value of 10.7 wt% in the zircon structure (Cuney & Brouand 1987). Where zoned, the rim contains distinctly less U than the core. As an example, in sample Zk5, one zoned crystal contains 3.99 wt%

TABLE 9. REPRESENTATIVE COMPOSITIONS OF ZIRCON FROM
THE YICHUN TOPAZ–LEPIDOLITE GRANITE, CHINA

Sample	1 Zk1	2 Zk5	3 Zk5	4 Zk6	5 Zk7	6 Zk7	7 Zk8	8 Zk9	9 Zk10	10 Zk12	11 Zk13
SiO_2 wt%	28.80	24.75	28.04	28.46	29.21	29.13	29.04	30.16	28.56	28.76	27.11
ZrO_2	55.42	52.49	43.89	53.87	51.47	57.31	53.01	56.85	48.26	54.94	50.99
HfO_2	5.37	4.53	21.98	6.46	14.58	4.96	9.80	8.24	4.85	5.38	4.54
P_2O_5	1.84	2.63	0.75	1.31	0.51	2.03	2.46	0.23	3.22	1.19	1.12
CaO	0.28	b.d.l.	0.11	0.21	0.11	0.45	0.41	0.03	0.39	0.07	b.d.l.
TiO_2	0.18	0.12	0.55	0.18	0.28	0.24	0.13	0.21	0.13	0.14	0.04
FeO	1.01	0.00	0.33	b.d.l.	0.05	b.d.l.	b.d.l.	b.d.l.	0.05	0.08	b.d.l.
UO_2	1.57	3.99	0.11	4.07	1.28	1.80	1.80	1.99	4.00	4.43	9.94
ThO_2	0.05	0.07	0.11	0.02	b.d.l.	0.00	0.02	0.14	0.27	0.08	0.69
MnO	0.58	0.43	b.d.l.	0.55	b.d.l.	0.58	0.51	0.29	0.87	0.91	0.01
Y_2O_3	0.92	1.48	0.47	0.75	b.d.l.	0.74	0.14	0.05	2.15	1.40	1.12
Al_2O_3	0.26	1.03	b.d.l.	0.33	0.04	0.22	0.54	0.37	0.34	0.29	b.d.l.
Total	96.29	93.23	98.59	96.20	97.53	97.46	97.85	98.57	93.07	97.67	95.56
Si *apfu*	0.937	0.861	0.976	0.947	0.980	0.934	0.940	0.979	0.948	0.942	0.941
Zr	0.879	0.891	0.745	0.874	0.842	0.896	0.837	0.900	0.781	0.877	0.863
Hf	0.050	0.045	0.218	0.061	0.140	0.045	0.091	0.076	0.046	0.050	0.045
P	0.051	0.078	0.022	0.037	0.014	0.055	0.068	0.006	0.090	0.033	0.033
Ca	0.010		0.004	0.007	0.004	0.016	0.014	0.001	0.014	0.002	
Ti	0.004	0.003	0.014	0.004	0.007	0.006	0.003	0.005	0.003	0.004	0.001
Fe	0.027	0.000	0.010		0.001				0.001	0.002	
U	0.011	0.031	0.001	0.030	0.010	0.013	0.013	0.014	0.030	0.032	0.077
Th	0.000	0.001	0.001	0.000		0.000	0.000	0.001	0.002	0.001	0.005
Mn	0.016	0.013		0.015		0.016	0.014	0.008	0.024	0.025	0.000
Y	0.026	0.045	0.014	0.022		0.021	0.004	0.002	0.063	0.040	0.034
Al	0.010	0.042		0.013	0.002	0.008	0.020	0.014	0.013	0.011	

b.d.l.: below detection limits. The structural formulae are calculated on the basis of four atoms of oxygen.

UO_2 in the core, but only 0.11 wt% at the rim (nos. 2 and 3, Table 9). In addition, in such uranium-enriched domains, the analytical total is usually clearly lower than 99.0 wt%, probably owing to the presence of H_2O in the structure, as is generally observed in partly metamict crystals. However, the content of Th is low, varying from below the detection limit to 0.69 wt% ThO_2, and mostly less than 0.40 wt%.

Yttrium

Yttrium varies from below the detection limit to 2.15 wt% Y_2O_3 (on average, 0.85 wt%: Table 9, Fig. 7c).

Phosphorus

The P content varies from 0.17 to 4.45 wt% P_2O_5, but is mostly greater than 1 wt% (Table 9, Fig. 7d). By comparison, zircon from P-poor granites contains generally less than 0.1 wt% P_2O_5. For example, zircon from the P-poor Suzhou granite, China, contains less than 0.5 wt% P_2O_5 (Wang *et al.* 1996).

THE Nb–Ta OXIDES

Minerals of the columbite group

Minerals of the columbite group are present throughout the drill hole, but most abundant in the upper part of the cupola. Petrographically, columbite is preferentially included as small tabular crystals of up to 50 μm in length in lepidolite, topaz, and albite in the lower part, but is interstitial to major minerals in the upper part of the section, where the crystals are characterized by complex zoning.

Compositions of columbite are presented in Table 10, and they are plotted in the columbite–tantalite quadrilateral in Figure 9. All points plot in the field of manganocolumbite – manganotantalite, with Ta/(Nb + Ta) varying from 0.14 to 0.95 and with a restricted Mn/(Fe + Mn) value, in the range 0.72 to 0.99. The crystals also contain minor amounts of Sn, Ti, and Sc. Tungsten is distinctly enriched in sample Zk1 at the top of the drill hole, up to 7.28 wt% WO_3 (Table 10).

The extent of chemical zoning was studied with back-scattered electron images, and confirmed by quantitative spot analysis. As shown by Belkasmi *et al.* (2000), the crystals exhibit two types of zonation: one with simple core-to-rim enrichment of tantalum (Fig. 10a, Table 11), another with a Ta-rich "inclusion-like" core with Ta/(Nb + Ta) of up to 0.9 (Fig. 10b, Table 11). In addition, we have demonstrated a replacement-induced patchy zoning in some crystals from the uppermost part of the section (Zk1, Fig. 10c, Table 11). Zonation of this type is characterized by an Fe-rich composition relative to the remainder of the crystal (Table 11). Patchy zoning is probably produced when columbite is subjected to alteration by later fluids.

From the point of view of vertical chemical variation of the columbite-group minerals, the Ta/(Nb + Ta) and Mn/(Fe + Mn) values along the vertical section have been compared (Fig. 8b). From bottom to top, the
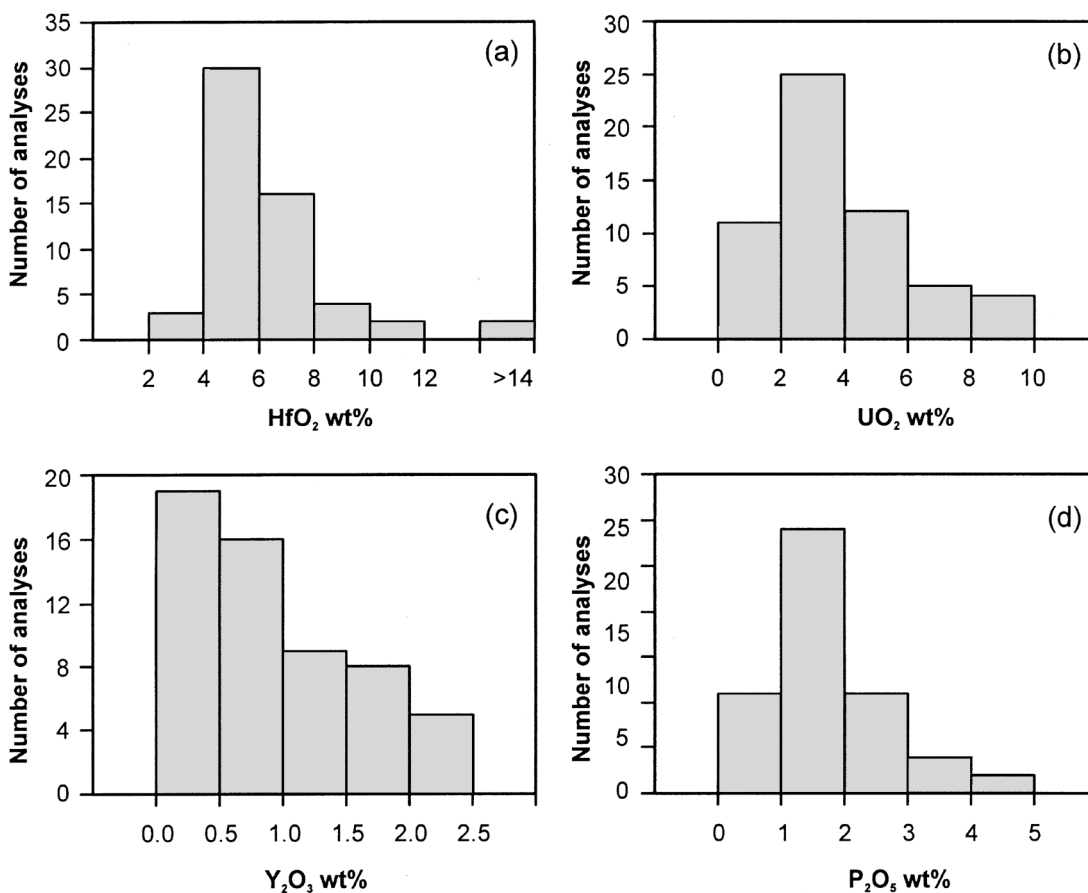
FIG. 7.   Histograms of HfO_2, UO_2, Y_2O_3 and P_2O_5 contents in zircon.

Mn/(Fe + Mn) value remains nearly constant (0.91–0.99), but enrichment in Fe has been observed at the uppermost part (Zk1), where the Mn/(Fe + Mn) value of the columbite decreases to 0.72 (FeO up to 5.76 wt%, Table 10). Enrichment in tungsten is also observed at the same depth (Fig. 8b). The figure also shows evidence of a progressive enrichment in Ta from the bottom to the middle part, but a weak decrease in Ta/(Nb + Ta) at the top.

Microlite

Microlite appears mainly in the middle part of the section (samples Zk5–Zk8), and is mostly associated with columbite–tantalite. Electron-microprobe data show that the microlite-group minerals are greatly variable in composition (Table 12). At the B site, tantalum is dominant relative to niobium; Ta_2O_5 varies from 67.15 to 79.89 wt% with an average of 75.77 wt%,

whereas Nb_2O_5 is much lower at up to 3.43 wt%, and 1.32 wt% on average; TiO_2 is present in minor amounts. The A site is mainly occupied by Na, Ca, U, Th, and Pb. Fluorine is present in significant amounts, up to 3.74 wt%. Compositions are recalculated assuming that the sum of B-site cations is 2 (Table 12).

Back-scattered electron images (BEI) show evidence of two generations of growth. Further electron-microprobe analyses reveals that the variation in color (a light core and a dark rim) is attributed to the variation in concentrations in the A-site cations. The A site is dominated by uranium in the core, whereas sodium and calcium occupy this site in the rim (Table 12). The U content attains 14.79 wt% UO_2 in the core of the crystals, corresponding to uranmicrolite (3C of Zk5, Table 12), whereas it varies in the range from 0 and 6.01 wt% at the rim. The abundance of uranium leads to metamictization of the microlite, as shown by the low total, about 90 wt%. The calculated structural formula of two
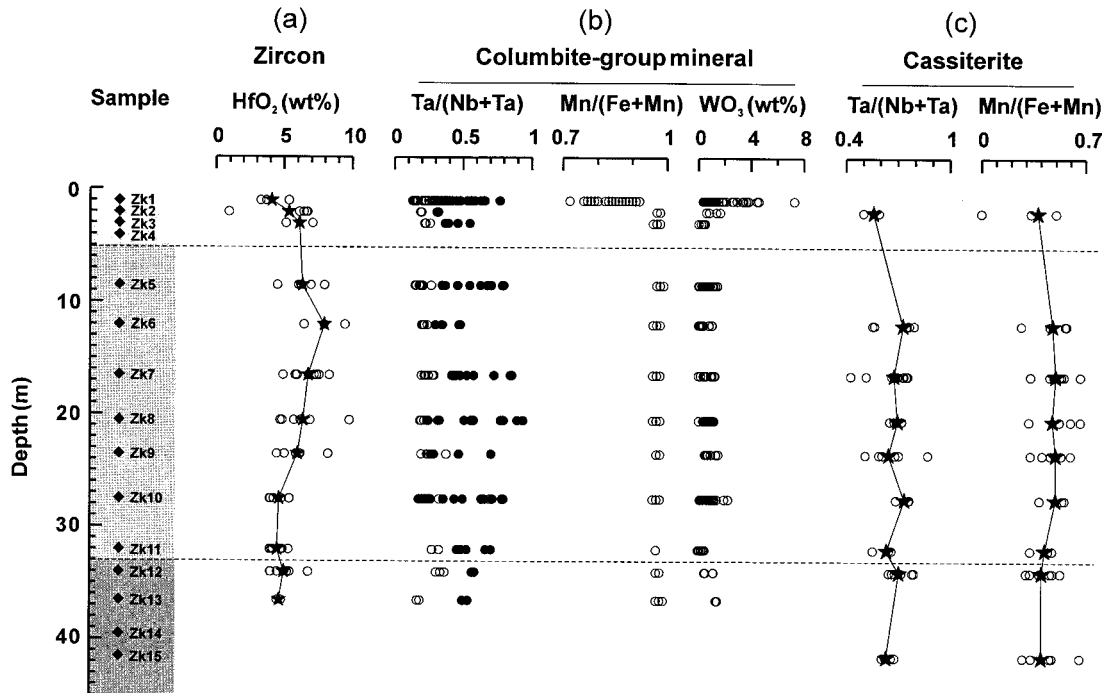
FIG. 8.   Chemical variations in zircon, columbite-group minerals and cassiterite with depth in the drill hole. (a) HfO_2 content of zircon. Stars: average HfO_2 contents. (b) Ta/(Nb + Ta), Mn/(Fe + Mn) values and WO_3 content of columbite-group minerals. Open circles: core, smaller solid circles: rim. (c) Ta/(Nb + Ta) and Mn/(Fe + Mn) values in cassiterite. Stars: average values.
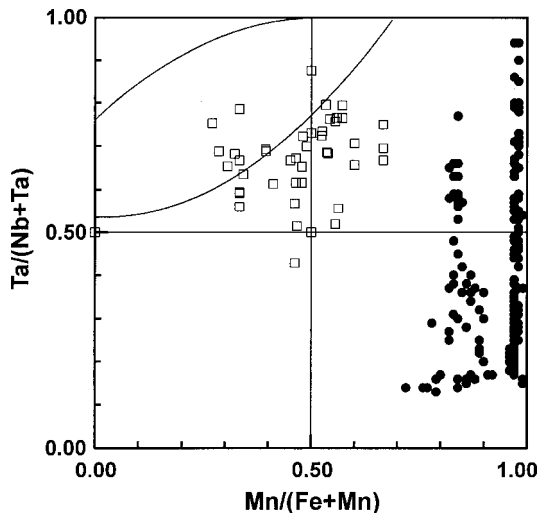

FIG. 9.   Composition of the columbite-group minerals (solid circles), and cassiterite (open squares) expressed in terms of the Mn/(Fe + Mn) *versus* Ta/(Nb + Ta) quadrilateral.

representative domains of microlite and uranmicrolite (No. 1 and 3C, Sample Zk5, Table 12) are given, respectively, as: $(Na_{1.008}Ca_{1.080}Fe_{0.004}U_{0.007}Sn_{0.019})$ $(Nb_{0.039}Ta_{1.961})O_{6.000}[F_{0.822}(OH)_{0.178}]$ and $(Na_{0.007}Ca_{0.009}Mn_{0.002}Fe_{0.001}U_{0.316}Sn_{0.032}Pb_{0.020})(Nb_{0.149}Ta_{1.849}Ti_{0.002})O_{6.000}(OH)_{1.000})$.

Wodginite-group minerals

To date, wodginite-group minerals have only been identified in granitic pegmatites (Tindle *et al.* 1998). However, they were identified by electron-microprobe analysis in our samples Zk8, Zk12, Zk13 and Zk14. Their occurrence in the Yichun topaz–lepidolite granite thus provides a first description of this mineral in granitic rocks. The wodginite-group minerals occur in association with columbite–tantalite and zircon. Our electron-microprobe data, plotted on a classification diagram (Ercit *et al.* 1992, Tindle *et al.* 1998), indicate that two subtypes exist: wodginite (SnO_2 up to 17.08 wt%) and titanowodginite (TiO_2 up to 8.47 wt%) (Table 13, Fig. 11). Titanowodginite is restricted to the lower part of the granite, where it coexists with
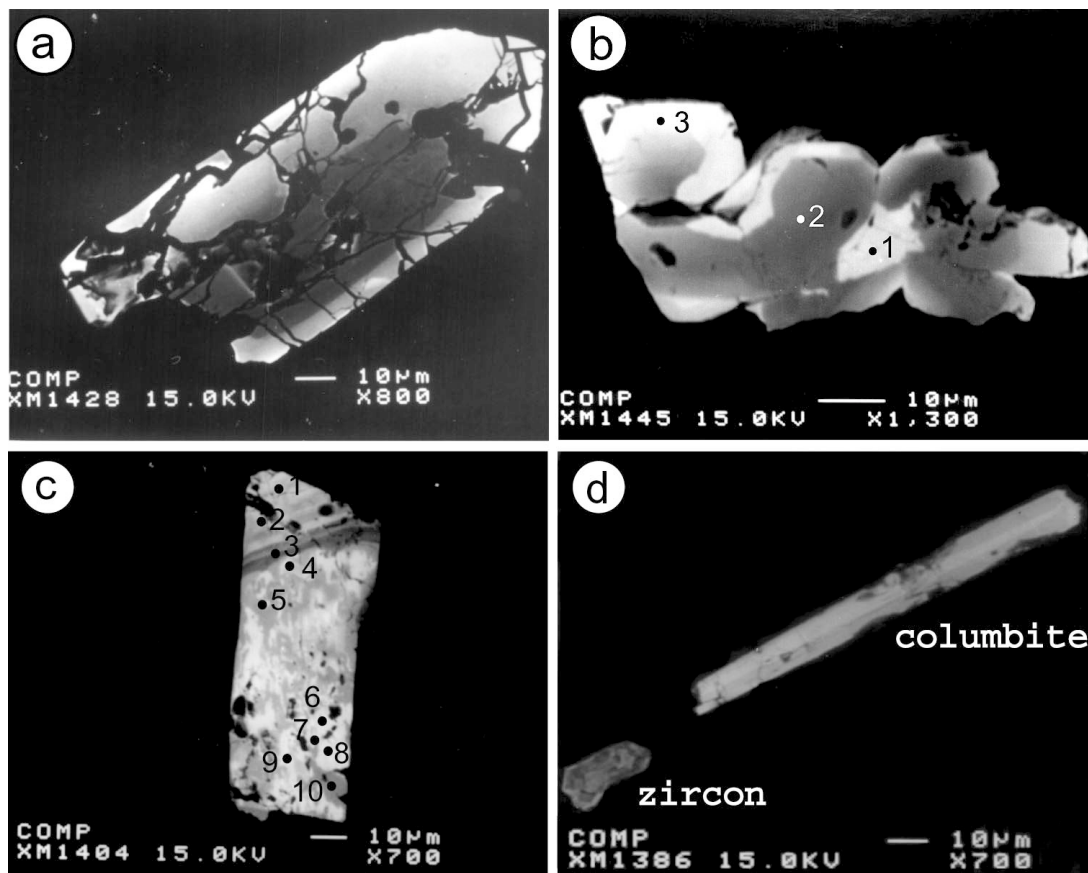
FIG. 10.   Back-scattered-electron images of columbite-group minerals. (a) Columbite with a core-to-rim enrichment in Ta. (b) Columbite with a Ta-rich "inclusion-like" core. (c) Columbite with replacement-induced patch zoning. (d) Needle-like crystal of columbite. Numbers in (b) and (c) correspond to those in Table 11.

wodginite (Fig. 12). In this case, wodginite and titanowodginite display very different SnO_2 and TiO_2 concentrations, suggestive of a possible miscibility-gap between $(Fe,Mn)Sn\ Ta_2O_8$ and $(Fe,Mn)TiTa_2O_8$ end-members, an aspect that is worthy of further study.

CASSITERITE

Most of the drill-hole samples contain cassiterite as the main mineral of tin (Table 14). Overall, the cassiterite has a limited range of compositions, and there is considerable overlap between any two facies of the section in FeO, MnO, Nb_2O_5, and Ta_2O_5 contents. Of these elements, Ta concentrations are highest and range from 0.60 to 3.38 wt% Ta_2O_5 in the lower facies, 0.23 to 5.49 wt% in the middle facies, and 0.09 to 1.8 wt% in the upper facies. Crystal-chemical calculation of cassiterite based on two atoms of oxygen per formula unit indicates that there is a good 1:2 correlation between Fe + Mn

and Nb + Ta, corresponding to the ideal coupled substitution $3\ Sn^{4+} \Leftrightarrow 2\ (Nb, Ta)^{5+} + (Fe, Mn)^{2+}$ in the cassiterite structure (Fig. 13). Plots of cassiterite in the columbite quadrilateral indicate that they are Ta-dominant, with a Ta/(Nb + Ta) value mostly in the range 0.50–0.90 (Fig. 9), the same as for cassiterite from granitic pegmatites (Černý & Ercit 1989). However, Ta/(Nb + Ta) and Mn/(Fe + Mn) both have the tendency to increase from the lower part to the middle part, and to decrease in the upper part of the section (Fig. 8c).

DISCUSSION

Mineralogical variation in the drill-hole section

According to the criteria of Taylor (1992), the Yichun topaz–lepidolite granite may be classified in the P-rich family of rare-element-enriched granites such as the Beauvoir granite, France (Cuney et al. 1992,

Raimbault *et al.* 1995), the Argemela granite, Portugal (Charoy & Noronha 1996), the evolved members of the South Mountain Batholith, Canada (Kontak *et al.* 1996), and the Podlesí stock, Czech Republic (Breiter *et al.* 1997). We recognize three petrographic facies of the topaz–lepidolite granite in the drilled section, with a trend from K-feldspar-rich facies at the lower part through albite-rich facies at the middle part, to an albite–K-feldspar-rich facies at the upper part. Corresponding to various facies in the section, the varieties, compositions, and abundance of minerals all changed at different depth. Although the phosphorus in magmatic minerals is mainly concentrated in feldspars in the

Yichun granite, like in other P-rich rare-element-enriched granites (London 1992, Kontak *et al.* 1996, Breiter *et al.* 1997), it is relatively less enriched in feldspars in the middle part, where primary amblygonite is abundant.

Ercit *et al.* (1992) suggested that as magmatic fractionation progresses in granitic pegmatites hosting wodginite-group minerals, there is an increase in Sn with respect to Ti prior to an increase in the chemical potential of Ta. In the Yichun drilled section, the distribution and composition of Ta–Nb–Sn–Ti oxide minerals also reflect their evolutionary pattern. Titanowodginite is only found in the lower part, whereas wodginite appears both at the lower part and at the middle part, and microlite is restricted to the middle part of the drill hole. Furthermore, columbite–tantalite displays a variable composition from the lower to the upper facies. The Ta/(Nb + Ta) value of columbite increases from the lower part to the middle part, and decreases in the upper part; whereas the Mn/(Fe + Mn) value of columbite is restricted to a narrow range, 0.91–0.99, except for the sharp decrease at the top of the drill hole. In addition, triplite occurs only at the top of the drill hole, consistent with the relative enrichment in Fe of columbite, which is formed in the latest facies of the granite, accompanied by an enrichment in tungsten (WO_3 content reaching up to 7.28 wt%). The Hf content of zircon shows a tendency to increase from the lower part to the middle part, but to decrease in the upper part of the section.
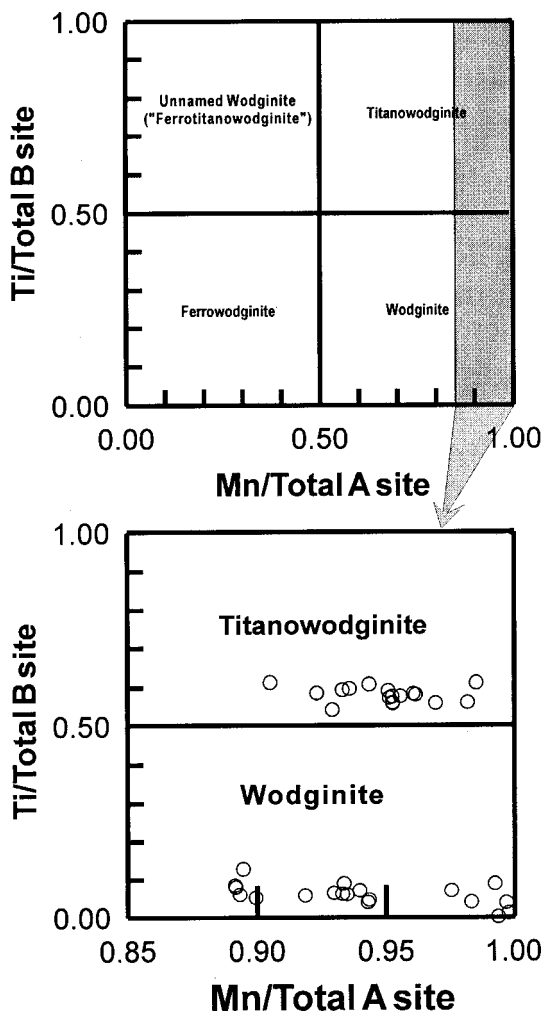
Magmatic-to-hydrothermal evolution of the Yichun topaz–lepidolite granite

The Yichun topaz–lepidolite granite is highly specialized, with economic concentrations of disseminated rare elements such as Li, Ta, Nb and Be. It shows an enrichment in alkalis and halogens. The minerals containing these rare elements are very sensitive to the physicochemical conditions of their environment of crystallization in the leucogranitic magma.

Belkasmi *et al.* (2000) distinguished two stages of evolution of the Yichun granitic complex based on chemistry of Nb–Ta–Sn oxide minerals. Firstly, fractional crystallization occurred in magma chamber at depth, which is reflected by the increase in the Ta/(Nb + Ta) value of Nb–Ta–Sn minerals from the muscovite–zinnwaldite granite to the lepidolite granite and the topaz–lepidolite granite. Secondly, magmatic differentiation occurred after intrusion of each stage, mainly reflected by increases in Ta/(Nb + Ta) and Mn/(Fe + Mn) during the growth of zoned crystals of columbite. Our findings provide further information on the crystallization history of the Yichun topaz–lepidolite granite.

Based on observation of variations of minerals in the vertical section, we propose, a "two-substage" model for the Yichun topaz–lepidolite granite. Magmatic dif-

FIG. 11.   Composition of wodginite-group minerals expressed in terms of the Mn/Total *A* site *versus* Ti/Total *B* site quadrilateral (after Ercit *et al.* 1992).
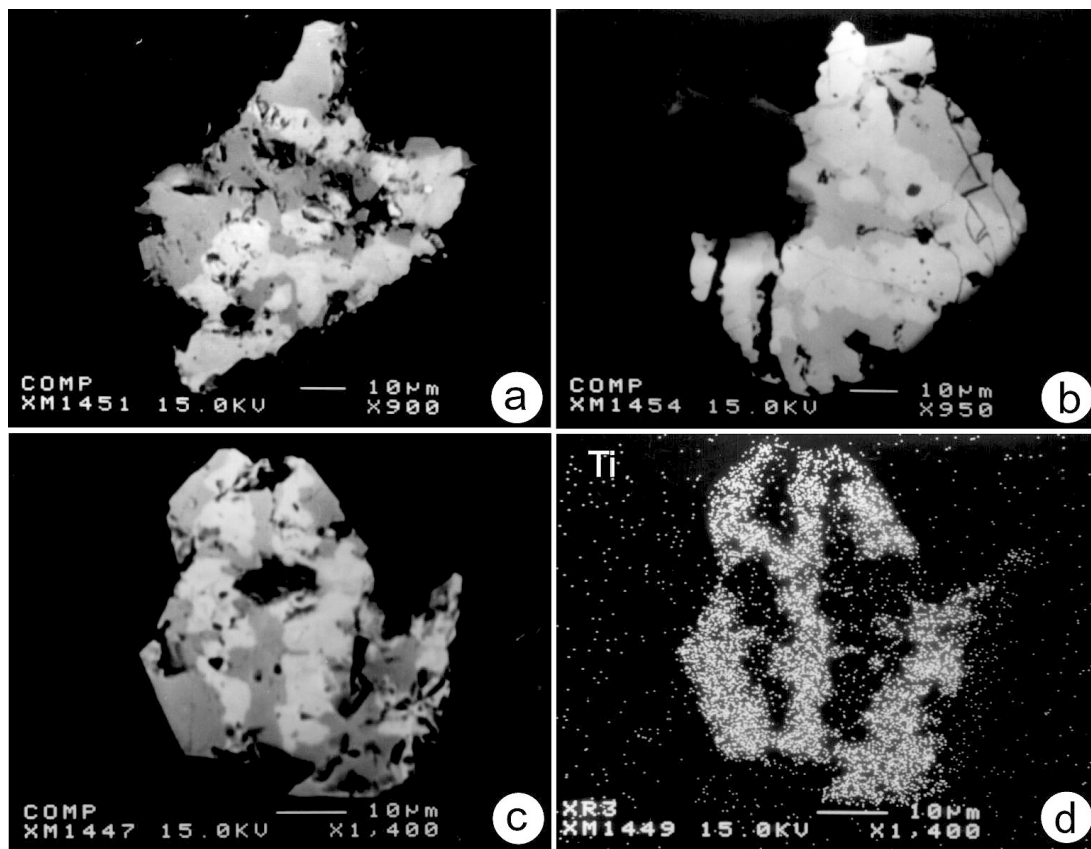
FIG. 12. Back-scattered-electron images (a, b, c) of coexisting wodginite (lighter) and titanowodginite. Ti X-ray image (d) corresponds to BSE image of (c).

TABLE 10. REPRESENTATIVE COMPOSITIONS OF COLUMBITE-GROUP MINERALS FROM THE YICHUN TOPAZ–LEPIDOLITE GRANITE, CHINA

	1 Zk1	2 Zk2	3 Zk3	4 Zk5	5 Zk6	6 Zk7	7 Zk8	8 Zk8	9 Zk9	10 Zk10	11 Zk11	12 Zk12	13 Zk13
TiO_2 wt%	1.52	0.09	0.17	0.08	0.07	0.61	0.53	0.12	0.75	1.58	0.44	0.21	0.51
Nb_2O_5	55.46	46.03	27.30	33.24	32.50	53.86	51.50	5.35	55.87	53.80	54.43	43.57	58.31
FeO	5.76	0.45	0.42	0.39	0.44	0.50	0.53	0.31	0.65	0.68	0.50	0.48	0.54
SnO_2	0.33	0.05	0.04	0.09	0.01	0.18	1.06	0.18	0.22	0.41	0.10	0.02	0.18
MnO	14.93	17.23	15.51	16.70	16.14	18.02	17.92	14.21	18.46	18.06	17.86	17.40	18.81
Ta_2O_5	15.55	34.22	55.15	47.66	49.38	24.77	27.33	78.83	23.15	22.08	25.26	36.60	20.38
WO_3	7.28	0.82	0.33	0.62	b.d.l.	1.00	1.06	0.36	1.37	2.31	0.29	1.19	1.43
Sc_2O_3	0.12	0.18	0.42	0.43	0.37	0.23	0.21	0.72	0.18	0.19	0.17	0.33	0.16
Total	100.94	99.05	99.35	99.23	98.92	99.18	99.24	100.07	100.64	99.10	99.05	99.78	100.32
Ti *apfu*	0.069	0.004	0.010	0.004	b.d.l.	0.029	0.025	0.008	0.034	0.074	0.021	0.010	0.023
Nb	1.518	1.368	0.893	1.052	1.038	1.529	1.479	0.187	1.552	1.513	1.547	1.300	1.608
Fe	0.292	0.024	0.026	0.023	0.026	0.026	0.028	0.021	0.033	0.035	0.026	0.026	0.027
Sn	0.008	0.001	0.001	0.003	0.000	0.005	0.004	0.006	0.005	0.010	0.003	0.001	0.004
Mn	0.767	0.960	0.951	0.992	0.966	0.960	0.966	0.984	0.962	0.953	0.951	0.974	0.973
Ta	0.256	0.612	1.085	0.908	0.949	0.423	0.472	1.751	0.387	0.384	0.432	0.657	0.338
W	0.114	0.014	0.006	0.011	0.000	0.016	0.017	0.008	0.022	0.037	0.005	0.020	0.023
Sc	0.006	0.010	0.026	0.026	0.023	0.013	0.012	0.051	0.009	0.010	0.009	0.019	0.008
$Mn^{\#}$	0.72	0.98	0.97	0.98	0.97	0.97	0.97	0.98	0.97	0.96	0.97	0.97	0.97
$Ta^{\#}$	0.14	0.31	0.55	0.46	0.48	0.22	0.24	0.90	0.20	0.20	0.22	0.34	0.17

Atomic ratios: $Mn^{\#}$ = Mn/(Fe + Mn), $Ta^{\#}$ = Ta/(Nb + Ta). b.d.l.: below detection limits.

TABLE 11. COMPOSITIONS OF SELECTED ZONED COLUMBITE CRYSTALS,
YICHUN TOPAZ–LEPIDOLITE GRANITE, CHINA

	Nb_2O_5	Ta_2O_5	FeO	MnO	TiO_2	SnO_2	WO_3	Sc_2O_3	Total	$Ta^\#$	$Mn^\#$

Simple progressive zoning. C: core, R: rim

1C	58.12	17.56	2.77	16.36	1.53	0.21	2.56	0.14	99.25	0.15	0.86
1R	38.59	41.95	2.40	15.84	0.25	b.d.l.	0.56	0.31	99.89	0.40	0.87
2C	47.53	30.25	2.57	15.78	0.65	0.16	1.54	0.24	98.72	0.28	0.86
2R	39.34	40.47	3.00	14.41	0.33	0.08	0.43	0.31	98.37	0.38	0.83
3C	54.10	23.77	0.68	18.57	0.59	0.11	0.88	0.18	98.87	0.21	0.97
3R	11.53	70.71	0.32	14.96	0.12	0.14	0.35	0.69	98.81	0.79	0.98
4C	54.56	23.24	0.68	18.83	0.47	0.10	0.81	0.17	98.85	0.20	0.97
4R	18.16	64.59	0.33	15.28	0.09	0.09	0.72	0.50	99.76	0.68	0.98
5C	48.89	31.70	0.42	17.95	0.08	0.16	0.49	0.25	99.93	0.28	0.98
5R	7.53	75.41	0.41	14.65	0.07	0.06	0.52	0.71	99.36	0.86	0.97

Zoning with Ta-rich "inclusion-like" core, Zk7 (Fig. 11b). 1: core, 3: rim

1	16.99	65.00	0.34	16.68	0.16	0.00	0.18	0.55	99.90	0.70	0.98
2	54.25	23.89	0.61	19.84	0.34	0.06	0.80	0.18	99.97	0.21	0.97
3	19.46	63.09	0.43	16.05	0.18	0.11	0.53	0.51	100.36	0.66	0.97

Patchy zoning, Zk1 (Fig. 11c)

1	45.29	29.95	4.08	14.46	2.17	0.25	3.61	0.15	99.97	0.29	0.78
2	47.25	25.47	3.37	15.12	3.19	0.29	4.43	0.17	99.28	0.25	0.82
3	58.95	15.76	3.33	16.70	2.05	0.18	2.68	0.21	99.85	0.14	0.84
4	23.63	56.72	2.91	14.09	0.77	0.18	1.18	0.43	99.92	0.59	0.83
5	41.29	38.86	2.48	16.03	0.20	b.d.l.	0.64	0.31	99.80	0.36	0.87
6	24.42	54.95	2.61	13.89	1.10	0.28	0.94	0.43	98.61	0.58	0.84
7	35.29	43.25	2.80	15.13	0.47	0.04	0.71	0.32	98.01	0.42	0.85
8	20.54	58.71	2.67	12.72	1.42	0.39	1.13	0.47	98.04	0.63	0.83
9	19.00	61.17	2.71	13.23	1.01	0.24	1.04	0.54	98.93	0.66	0.83
10	40.93	39.86	3.30	15.23	0.68	0.05	1.17	0.31	101.52	0.37	0.83

Atom ratios: $Mn^\# = Mn/(Fe + Mn)$; $Ta^\# = Ta/(Nb + Ta)$. b.d.l.: below detection limits. The compositions are expressed in wt%.

TABLE 12. REPRESENTATIVE COMPOSITIONS OF MICROLITE FROM
THE YICHUN TOPAZ–LEPIDOLITE GRANITE, CHINA

	Zk5 3C	4R	4C	Zk6 1R	1C	2	Zk7 3R	3C	1 1	2 2	3R
Nb_2O_5 wt%	0.93	2.67	1.38	3.43	0.68	1.56	0.78	1.44	0.66	0.72	1.47	0.62	1.40
Ta_2O_5	77.66	67.44	76.13	70.82	78.82	73.91	78.30	73.78	79.00	79.10	74.16	79.11	73.13
TiO_2	b.d.l.	0.03	b.d.l.	0.03	b.d.l.	b.d.l.	b.d.l.	b.d.l.	b.d.l.	0.06	0.04	b.d.l.	b.d.l.
Na_2O	5.60	0.30	4.56	0.04	6.66	5.27	6.79	4.87	6.79	6.49	5.04	6.73	5.21
CaO	10.86	4.63	8.41	0.09	10.91	7.01	10.82	8.20	11.02	10.82	7.57	10.85	7.64
MnO	b.d.l.	0.05	0.06	0.03	0.03	b.d.l.	0.05	0.03	b.d.l.	b.d.l.	0.03	0.02	0.02
FeO	0.05	b.d.l.	0.01	0.01	0.02	b.d.l.	0.03	b.d.l.	b.d.l.	0.03	b.d.l.	0.02	b.d.l.
UO_2	0.34	13.39	6.01	14.79	b.d.l.	8.47	0.16	6.21	0.08	0.22	7.66	b.d.l.	7.90
ThO_2	0.02	b.d.l.	0.02	b.d.l.	0.03	0.07	0.01	b.d.l.	b.d.l.	b.d.l.	b.d.l.	0.06	0.14
SnO_2	0.51	0.87	0.49	0.83	0.43	0.56	0.50	0.73	0.45	0.45	0.69	0.45	0.72
PbO	b.d.l.	0.26	0.16	0.78	b.d.l.	0.39	b.d.l.	0.25	0.07	b.d.l.	b.d.l.	b.d.l.	0.11
F	2.80	1.31	1.69	b.d.l.	3.08	1.90	2.75	2.18	2.33	1.77	0.65	1.19	0.15
2F=O	-1.18	-0.55	-0.71		-1.29	-0.80	-1.16	-0.92	-0.98	-0.74	-0.27	-0.50	-0.06
Total	97.59	90.4	98.21	90.85	99.35	98.32	99.02	96.76	99.43	98.93	97.03	98.54	96.37
Nb *apfu*	0.039	0.123	0.058	0.149	0.028	0.068	0.033	0.063	0.027	0.030	0.064	0.026	0.062
Ta	1.961	1.874	1.942	1.849	1.972	1.932	1.967	1.937	1.973	1.966	1.933	1.974	1.938
Ti		0.002		0.002						0.004	0.003		
ΣB	2.000	2.000	2.000	2.000	2.000	2.000	2.000	2.000	2.000	2.000	2.000	2.000	2.000
Na	1.008	0.059	0.829	0.007	1.188	0.982	1.216	0.911	1.209	1.150	0.937	1.197	0.984
Ca	1.080	0.507	0.845	0.009	1.075	0.722	1.071	0.848	1.084	1.059	0.777	1.067	0.798
Mn		0.004	0.005	0.002	0.002		0.004	0.002			0.002	0.002	0.002
Fe	0.004	0.000	0.001	0.001	0.002		0.002			0.002		0.002	
U	0.007	0.304	0.125	0.316		0.181	0.003	0.133	0.002	0.004	0.163		0.171
Th	0.000		0.000		0.001	0.002	0.000					0.001	0.003
Sn	0.019	0.035	0.018	0.032	0.016	0.021	0.018	0.028	0.016	0.016	0.026	0.016	0.028
Pb		0.007	0.004	0.020	0.000	0.010	0.000	0.006	0.002	0.000	0.000	0.000	0.003
ΣA	2.118	0.918	1.827	0.388	2.283	1.918	2.315	1.930	2.312	2.232	1.906	2.285	1.989
F	0.822	0.423	0.501		0.896	0.577	0.803	0.665	0.676	0.512	0.197	0.345	0.046

b.d.l.: below detection limits; C: core, R: rim. The structural formulae are calculated assuming Σ cations at the B site is equal to 2.

ferentiation occurred in the first substage of crystallization of the magma, corresponding to the lower and middle parts of the granite. Increases in Ta/(Nb + Ta) and Mn/(Fe + Mn) of Nb–Ta oxide minerals and in Hf content of zircon with differentiation of the magma are well known both in granitic pegmatites (Černý *et al.* 1986, Mulja *et al.* 1996, Tindle & Breaks 2000) and in rare-element-enriched granites (Wang *et al.* 1987, 1992, 1996, 1997, Belkasmi *et al.* 2000). In fact, columbite and zircon from the Yichun topaz–lepidolite granite display progressive increases in Ta/(Nb + Ta) and Hf content, respectively, from the lower part to the middle part of the drill hole, suggestive of magmatic differentiation at the beginning of crystallization after the intrusion of the magma at a shallow level. Crystallization is followed by increase in volatile contents, as shown in Figure 14: F and P contents increase from the lower part to the middle part. The high fluoride concentration and increased μHF modified the mineralogy of Nb, Ta oxides strongly in favor of microlite and also led to the crystallization of phosphates (Černý 1989). The presence of primary microlite, amblygonite, and fluorapatite in the middle facies of the Yichun topaz–lepidolite granite are strong indicators of advanced fractionation. In addition to this type of enrichment in P in the middle facies with magmatic crystallization, there is also substantial secondary enrichment. Inclusions of secondary apatite are related to subsolidus recrystallization of P-bearing K-feldspar in presence of a fluid phase. Cs-rich lepidolite, occurring as a rim on earlier lepidolite, reflects the existence of Cs-rich fluid at the middle to upper part. Also, the occurrence of herderite implies a beryllium-rich late-magmatic fluid at the lower to middle part. The effect of fluids on the Yichun granite was also observed in the tetrad shape of the *REE* patterns.

At the second substage, the crystallization of the upper part of the granite is influenced by fluid, probably originating from the surrounding mica schist. The decrease in Ta/(Nb + Ta) of columbite and in Hf contents of zircon indicates a different environment of growth. At the contact of the magma with the surrounding rocks, in particular, the columbite shows a drastic decrease in Mn/(Fe + Mn). The enrichment in Fe and also in W is probably due to the fluids derived from the wallrock, which is Precambrian mica schist enriched in Fe and W. Accordingly, the lepidolite of the uppermost sample contains abundant Fe. At the top of the Beauvoir granite, knots of cassiterite + columbite have been found, in which columbite and lepidolite exhibit patchy zoning with enrichment in Fe relative to Mn (Monier *et al.* 1987, Fonteilles 1987, Wang 1988). A similar phenomenon has also been observed in the Yichun topaz–lepidolite granite, and patchy zoning characterizes columbite in the upper part of the section.

TABLE 13. COMPOSITION OF WODGINITE-GROUP MINERALS FROM THE YICHUN TOPAZ–LEPIDOLITE GRANITE, CHINA

	Wodginite					Titanowodginite				
	Zk8	Zk12		Zk13		Zk12				
n	5	12	21	5	6	13	17	20	24	33
Nb₂O₅ wt%	3.09	5.04	4.46	4.99	6.79	8.07	11.15	9.34	9.21	10.14
Ta₂O₅	69.56	64.26	64.96	66.33	62.26	66.04	65.55	65.64	64.86	64.85
WO₃	0.41	0.26	0.02	0.24	0.41	0.17	0.02	0.35	0.18	0.22
Fe₂O₃	1.54	1.11	0.98	1.45	0.80	0.68	0.72	0.70	0.72	0.23
TiO₂	b.d.l.	0.74	0.73	0.71	1.62	7.70	8.00	7.92	7.55	8.12
SnO₂	13.85	15.78	16.99	14.36	16.32	5.05	3.73	4.34	5.07	4.40
Sc₂O₃	0.49	0.47	0.32	0.50	0.45	0.44	0.50	0.47	0.48	0.47
FeO	0.07	0.72	1.19	0.91	1.21	0.57	0.56	0.45	0.36	0.74
MnO	10.43	10.25	9.86	10.11	10.15	11.04	11.18	11.20	11.30	10.62
Total	99.43	98.62	99.52	99.58	100.00	99.76	101.41	100.41	99.72	99.79
C site										
Nb *apfu*	0.608	0.980	0.863	0.961	1.277	1.443	1.930	1.646	1.638	1.791
^{C}Ta	7.346	6.992	7.134	7.013	6.679	6.540	6.068	6.319	6.344	6.187
W	0.046	0.028	0.003	0.026	0.044	0.017	0.002	0.036	0.018	0.022
Total	8.000	8.000	8.000	8.000	8.000	8.000	8.000	8.000	8.000	8.000
B site										
^{B}Ta	0.900	0.522	0.429	0.679	0.370	0.562	0.757	0.639	0.595	0.701
Fe³⁺	0.507	0.359	0.315	0.467	0.251	0.202	0.207	0.205	0.214	0.068
Ti	0.000	0.240	0.236	0.228	0.508	2.290	2.301	2.321	2.234	2.385
Sn	2.406	2.705	2.900	2.441	2.709	0.796	0.569	0.675	0.795	0.686
Sc	0.187	0.175	0.120	0.185	0.162	0.151	0.165	0.160	0.163	0.160
Total	4.000	4.000	4.000	4.000	4.000	4.000	4.000	4.000	4.000	4.000
A site										
Fe²⁺	0.025	0.260	0.426	0.323	0.421	0.189	0.180	0.147	0.118	0.240
Mn	3.848	3.731	3.574	3.650	3.578	3.698	3.626	3.697	3.763	3.512
Total	3.873	3.991	4.001	3.973	3.999	3.886	3.806	3.845	3.882	3.752

Fe^{2+} / Fe^{3+} is calculated following the method of Ercit *et al.* (1992). b.d.l.: below detection limits The structural formulae are calculated on the basis of thirty-two atoms of oxygen. *n*: number of electron-microprobe analyses made.
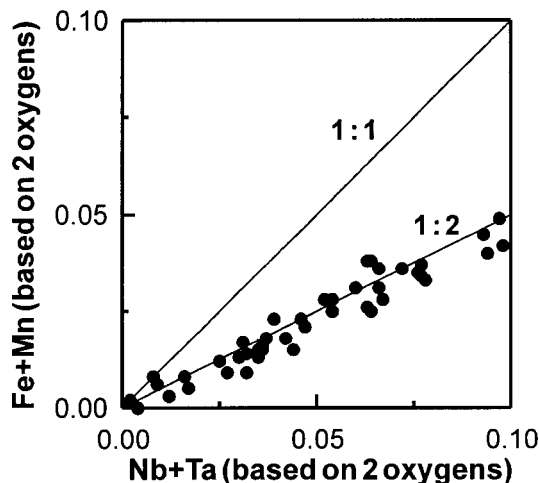

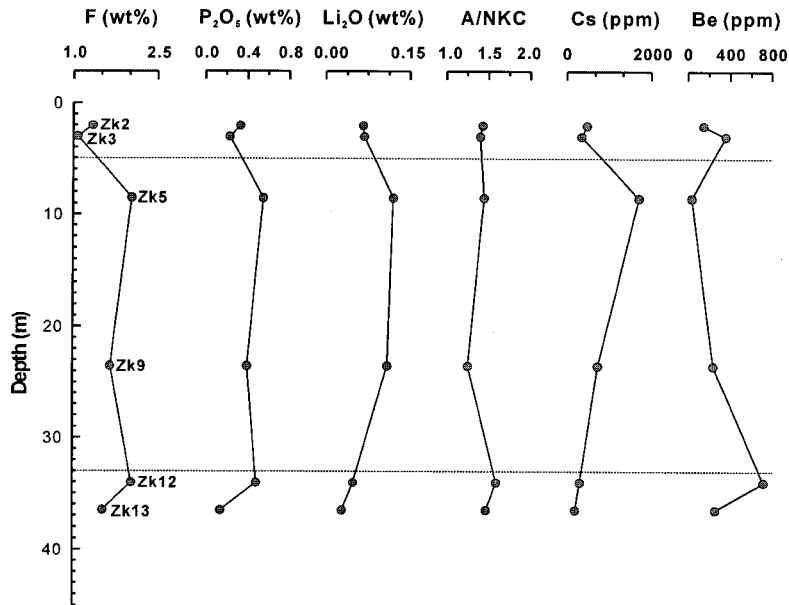FIG. 13. Covariation of Ta/(Nb + Ta) and Mn/(Fe + Mn) in cassiterite.

FIG. 14. Variations in F, P$_2$O$_5$, LiO$_2$ and A/NKC with depth in the drill hole. A/NKC: Al$_2$O$_3$ / (Na$_2$O + K$_2$O + 2CaO) (molar).

Comparison with the Beauvoir granite, Massif Central, France

The Yichun topaz–lepidolite granite and the Beauvoir topaz–lepidolite granite (France) are typical of rare-element-enriched granites in the world. The Beauvoir granite is divided, from the top to the bottom over its 800 m interval, into three facies: BI, BII, BIII (Cuney *et al.* 1992, Raimbault *et al.* 1995). Although there are many similarities, some characteristics are also distinctive in these two granites. Therefore, it is interesting to make comparison in mineralogy between them.

Albite, quartz, K-feldspar, and lepidolite are the major rock-forming minerals both in the Yichun topaz–lepidolite granite and in the Beauvoir granite (Raimbault *et al.* 1995). High phosphorus contents are typical of feldspars from two granites. In the Beauvoir granite, the P contents of feldspars reach up to 1.07 wt% P$_2$O$_5$ (London *et al.* 1990, London 1992), slightly higher that those of feldspars from the Yichun topaz–lepidolite granite. Enrichment in P is also marked by abundant amblygonite occurring as an interstitial mineral between major minerals in the two granites compared.

The rare-element-enriched minerals include columbite–tantalite, microlite, cassiterite and zircon in the Beauvoir topaz–lepidolite granite; in addition to these minerals, wodginite-group minerals are found in the Yichun granite. The Nb–Ta minerals of the Beauvoir granite illustrate the paragenetic sequence from ferrocolumbite through manganocolumbite to mangano-

TABLE 14. COMPOSITION OF CASSITERITE FROM THE YICHUN TOPAZ–LEPIDOLITE GRANITE, CHINA

Sample n	Zk2 3	Zk6 5	Zk7 10	Zk8 4	Zk9 6	Zk10 3	Zk11 3	Zk12 6	Zk15 5
Nb$_2$O$_5$ wt%	0.32	0.78	0.62	0.71	0.48	0.85	0.69	0.72	0.64
Ta$_2$O$_5$	0.72	3.53	2.15	2.62	1.41	4.04	2.06	2.92	1.86
FeO	0.12	0.37	0.22	0.27	0.17	0.39	0.29	0.37	0.30
MnO	0.07	0.35	0.23	0.26	0.15	0.38	0.23	0.25	0.20
TiO$_2$	0.27	0.25	0.12	0.35	0.18	0.16	0.42	0.22	0.34
SnO$_2$	94.46	92.24	94.70	93.21	94.77	91.16	95.61	94.26	96.99
WO$_3$	0.35	0.01	0.05	b.d.l.	0.04	0.02	0.42	0.01	0.44
Total	96.30	97.53	98.10	97.41	97.19	97.01	99.71	98.74	100.78
Nb *apfu*	0.004	0.009	0.007	0.008	0.006	0.010	0.008	0.008	0.007
Ta	0.005	0.025	0.015	0.018	0.010	0.028	0.014	0.020	0.013
Fe	0.003	0.008	0.005	0.006	0.004	0.008	0.006	0.008	0.006
Mn	0.002	0.008	0.005	0.006	0.003	0.008	0.005	0.005	0.004
Ti	0.005	0.005	0.002	0.007	0.003	0.003	0.008	0.004	0.006
Sn	0.978	0.945	0.965	0.954	0.973	0.940	0.955	0.954	0.959
W	0.002	0.000	0.000		0.000	0.000	0.003	0.000	0.003
Total	0.999	1.000	0.999	0.999	0.999	0.997	0.999	0.999	0.998

b.d.l.: below detection limits. The structural formulae are calculated on the basis of two atoms of oxygen. *n*: number of electron-microprobe analyses made.

tantalite, whereas the composition of the columbite–tantalite-group minerals of the Yichun granite changes along the restricted vertical profile [0.72 < Mn/(Fe + Mn) < 0.99, 0.14 < Ta/(Nb + Ta) < 0.95] from manganocolumbite to manganotantalite.

Cassiterite is abundant throughout the Beauvoir granite, particularly in the apical facies. Inclusions of manganocolumbite, commonly oriented and attributed

to exsolution, have been observed in the cassiterite in the middle to lower facies, but are absent in those of the upper facies. Overall, the Nb and Ta contents of cassiterite also increase upward, then decrease in the apical part; this pattern is probably due to late-magmatic fluids in the upper facies (Wang *et al.* 1987). In the Yichun lepidolite granite, cassiterite is less abundant and free of columbite inclusions, but yet the Nb, Ta contents in cassiterite similarly increase from the lower part to the middle part, and decrease in the upper part. A highly Hf-enriched rim is observed on zircon both at Beauvoir and at Yichun; in fact, hafnian zircon is one of accessory minerals typical of rare-element-enriched granites.

A comparative study demonstrates that rare-element-enriched granites such as at Yichun and Beauvoir display similar mineralogical compositions. P-bearing feldspars is a sign of high-P granites. Overall, accessory minerals containing the rare elements indicate that this type of granite crystallized in an evolving magmatic-to-hydrothermal system, and shows characteristics of granitic pegmatites (Wang *et al.* 1992).

References

Bea, F. (1996): Residence of REE, Y, Th and U in granites and crustal protoliths: implications for the chemistry of crustal melts. *J. Petrol.* **37**, 521-552.

_____, Pereira, M.D., Corretgé, L.G. & Fershtater, G.B. (1994): Differentiation of strongly peraluminous, perphosphorous granites: the Pedrobernardo pluton, central Spain. *Geochim. Cosmochim. Acta* **58**, 2609-2627.

Belkasmi, M., Cuney, M., Pollard, P.J. & Bastoul, A. (2000): Chemistry of the Ta–Nb–Sn–W oxide minerals from the Yichun rare metal granite (SE China): genetic implications and comparison with Moroccan and French Hercynian examples. *Mineral. Mag.* **64**, 507-523.

_____, _____, Raimbault, L. & Pollard, P.J. (1991): Chemistry of the micas from the Yashan rare metal granite (SE China). A comparison with Variscan examples. *In* Source, Transport and Deposition of Metals (M. Pagel & J. Leroy, eds.). Balkema, Rotterdam, The Netherlands.

Breiter, K., Frýda, J., Seltmann, R. & Thomas, R. (1997): Mineralogical evidence for two magmatic stages in the evolution of an extremely fractionated P-rich rare-metal granite: the Podlesí stock, Krušné Hory, Czech Republic. *J. Petrol.* **38**, 1723-1739.

Černý, P. (1989): Characteristics of pegmatite deposits of tantalum. *In* Lanthanides, Tantalum and Niobium (P. Möller, P. Černý & F. Saupé, eds.). Springer-Verlag, Berlin, Germany (195-239).

_____ & Ercit, T.S. (1989): Mineralogy of niobium and tantalum: crystal chemical relationships, paragenetic aspects and their economic implications. *In* Lanthanides, Tantalum and Niobium (P. Möller, P. Černý & F. Saupé, eds.). Springer-Verlag, Berlin, Germany (27-79).

_____, Goad, B.E., Hawthorne, F.C. & Chapman, R. (1986): Fractionation trends of the Nb- and Ta-bearing oxide minerals in the Greer Lake pegmatitic granite and its pegmatite aureole, southeastern Manitoba. *Am. Mineral.* **71**, 501-517.

Charoy, B. (1999): Beryllium speciation in evolved granitic magmas: phosphates versus silicates. *Eur. J. Mineral.* **11**, 135-148.

_____ & Noronha, F. (1996): Multistage growth of a rare-element, volatile-rich microgranite at Argemela (Portugal). *J. Petrol.* **37**, 73-94.

Correia Neves, J.M., Lopes Nunes, J.E. & Sahama, T.G. (1974): High hafnian members of the zircon–hafnon series from the granite pegmatites of Zambezia, Mozambique. *Contrib. Mineral. Petrol.* **48**, 73-80.

Cuney, M. & Brouand, M. (1987): Minéralogie et géochimie de U et Th dans le granite de Beauvoir et les micaschistes encaissants. *Géol. France* **2–3**, 247-257.

_____, Marignac, C. & Weisbrod, A. (1992): The Beauvoir topaz–lepidolite albite granite (Massif Central, France): the disseminated magmatic Sn–Li–Ta–Nb–Be mineralization. *Econ. Geol.* **87**, 1766-1794.

Ercit, T.S., Černý, P. & Hawthorne, F.C. (1992): The wodginite group. III. Classification and new species. *Can. Mineral.* **30**, 633-638.

Fonteilles, M. (1987): La composition chimique des micas lithinifères (et autres minéraux) des granites d'Echassières comme image de leur évolution magmatique. *Géol. France* **2–3**, 149-178.

Förster, H.-J. (1998a): The chemical composition of REE–Y–Th–U-rich accessory minerals in peraluminous granites of the Erzgebirge–Fichtelgebirge region, Germany. I. The monazite-(Ce)–brabantite solid solution series. *Am. Mineral.* **83**, 259-272.

_____ (1998b): The chemical composition of REE–Y–Th–U-rich accessory minerals in peraluminous granites of the Erzgebirge–Fichtelgebirge region, Germany. II. Xenotime. *Am. Mineral.* **83**, 1302-1315.

Hinton, R.W. & Paterson, B.A. (1994): Crystallization history of granitic magma: evidence from trace element zoning. *Mineral. Mag.* **58A**, 416-417.

Kontak, D.J., Martin, R.F. & Richard, L. (1996): Patterns of phosphorus enrichment in alkali feldspar, South Mountain Batholith, Nova Scotia, Canada. *Eur. J. Mineral.* **8**, 805-824.

LONDON, D. (1992): Phosphorus in S-type magmas: the P_2O_5 content of feldspars from peraluminous granites, pegmatites, and rhyolites. *Am. Mineral.* **77**, 126-145.

_____, ČERNÝ, P., LOOMIS, J.L. & PAN, J.J. (1990): Phosphorus in alkali feldspars of rare-element granitic pegmatites. *Can. Mineral.* **28**, 771-786.

_____, MORGAN, G.B., VI, BABB, H.A. & LOOMIS, J.L. (1993): Behavior and effects of phosphorus in the system $Na_2O–K_2O–Al_2O_3–SiO_2–P_2O_5–H_2O$ at 200 MPa (H_2O). *Contrib. Mineral. Petrol.* **113**, 450-465.

_____, WOLF, M.B., MORGAN, G.B., VI & GARRIDO, M.G. (1999): Experimental silicate–phosphate equilibria in peraluminous granitic magmas, with a case study of the Albuquerque batholith at Tres Arroyos, Badajoz, Spain. *J. Petrol.* **40**, 215-240.

LU, H.Z., SHI, J.X. & YU, C.M. (1975): Temperatures of petrogenesis and metallogenesis for a certain tantalum–niobium-bearing granite. *Geochimica* **3**, 210-221 (in Chinese).

MASUDA, A., KAWAKAMI, O., DOHMOTO, Y. & TAKENAKA, T. (1987): Lanthanide tetrad effects in nature: two mutually opposite types, W and M. *Geochem. J.* **21**, 119-124.

MONIER, G., CHAROY, B., CUNEY, M., OHNENSTETTER, D. & ROBERT, J.-L. (1987): Evolution spatiale et temporelle de la composition des micas du granite albitique à topaz–lépidolite de Beauvoir. *Géol. France* **2–3**, 179-188.

MULJA, T., WILLIAMS-JONES, A.E., MARTIN, R.F. & WOOD, S.A. (1996): Compositional variation and structural state of columbite–tantalite in rare-element granitic pegmatites of the Preissac–Lacorne batholith, Quebec, Canada. *Am. Mineral.* **81**, 146-157.

POLLARD, P.J. & TAYLOR, R.P. (1991): Petrogenetic and metallogenetic implications of the occurrence of topaz–Li-mica granite at the Yichun Ta–Nb–Li mine, Jiangxi Province, South China, *In* Source, Transport and Deposition of Metals (M. Pagel & J. Leroy, eds.). Balkema, Rotterdam, The Netherlands (789-791).

RAIMBAULT, L., CHAROY, B., CUNEY, M. & POLLARD, P.J. (1991): Comparative geochemistry of Ta-bearing granites. *In* Source, Transport and Deposition of Metals (M. Pagel & J. Leroy, eds.). Balkema, Rotterdam, The Netherlands (793-796).

_____, CUNEY, M., AZENCOTT, C., DUTHOU, J.L. & JORN, J.L. (1995): Geochemical evidence for a multistage magmatic genesis of Ta–Sn–Li mineralization in the granite at Beauvoir, French Massif Central. *Econ. Geol.* **90**, 548-576.

ROSENBERG, P.E. (1972): Compositional variations in synthetic topaz. *Am. Mineral.* **57**, 169-187.

SCHWARTZ, M.O. (1992): Geochemical criteria for distinguishing magmatic and metasomatic albite-enrichment in granitoids – examples from the Ta–Li granite Yichun (China) and the Sn–W deposit Tikus (Indonesia). *Mineral. Deposita* **27**, 101-108.

TAYLOR, R.P. (1992): Petrological and geochemical characteristics of the Pleasant Ridge zinnwaldite–topaz garnite, southern New Brunswick, and comparisons with other topaz-bearing felsic rocks. *Can. Mineral.* **30**, 895-921.

TINDLE, A.G. & BREAKS, F.W. (1998): Oxide minerals of the Separation Rapids rare-element granitic pegmatite group, northwestern Ontario. *Can. Mineral.* **36**, 609-636.

_____ & _____ (2000): Columbite–tantalite mineral chemistry from rare-element granitic pegmatites: Separation Lake area, N.W. Ontario, Canada. *Mineral. Petrol.* **70**, 165-198.

_____, _____ & WEBB, P.C. (1998): Wodginite-group minerals from the Separation Rapids rare-element granitic pegmatite group, northwestern Ontario. *Can. Mineral.* **36**, 637-658.

WANG, RU CHENG (1988): *Etude minéralogique et cristallo-chimique de cassitérite, niobo-tantalates et minéraux disséminés du granite de Beauvoir (Allier); implications métallogéniques*. Thèse de doctorat, Univ. Paul Sabatier, Toulouse, France.

_____, FONTAN, F. & MONCHOUX, P. (1992): Minéraux disseminés comme indicateurs du caractère pegmatitique du granite de Beauvoir, Massif d'Echassières, Allier, France. *Can. Mineral.* **30**, 763-770.

_____, _____ & _____ (1987): Interrelations et évolution comparée de la cassitérite et des niobotantalates dans les différents faciès du granite de Beauvoir. *Géol. France* **2–3**, 237-245.

_____, _____, XU, SHIJIN, CHEN, XIAOMING & MONCHOUX, P. (1996): Hafnian zircon from the apical part of the Suzhou granite, China. *Can. Mineral.* **34**, 1001-1010.

_____, _____, _____, _____ & _____ (1997): The association of columbite, tantalite and tapiolite in the Suzhou granite, China. *Can. Mineral.* **35**, 699-706.

WARK, D.A. & MILLER, C.F. (1993): Accessory mineral behavior during differentiation of a granite suite: monazite, xenotime, and zircon in the Sweetwater Wash pluton, southeastern California, U.S.A. *Chem. Geol.* **110**, 49-67.

YIN, L. (1988): *Contrasting of Mineralization Characteristics of W, Sn, Ta and Nb Deposits Related to Transformation Type Granites in South China*. Ph.D. thesis, Nanjing University, Nanjing, China.

_____, POLLARD, P.J., HU, SHOUXI & TAYLOR, R.G. (1995): Geologic and geochemical characteristics of the Yichun Ta–Nb–Li deposit, Jiangxi Province, South China. *Econ. Geol.* **90**, 577-585.

YIN, LIN, ZHU, J.C. & HU, SHOUXI (1993): Multiple-staged granite evolution and Ta–Nb mineralization in South China. *J. Southeast Asian Earth Sci.* **8**, 321-328.